Geophys. J. Int. (2005) **161,** 491–506 doi: 10.1111/j.1365-246X.2005.02609.x

The rotational stability of an ice-age earth

Jerry X. Mitrovica,[1] John Wahr,[2] Isamu Matsuyama[3] and Archie Paulson[2]

[1] *Department of Physics, University of Toronto,* 60 *St George Street, Toronto, Canada* M5S 1A7. *E-mail: jxm@physics.utoronto.ca*
[2] *Department of Physics, Campus Box* 390*, University of Colorado, Boulder,* CO 80309*, USA*
[3] *Department of Astronomy & Astrophysics, University of Toronto,* 60 *St George Street, Toronto, Canada* M5S 3H8

Accepted 2005 February 8. Received 2005 February 2; in original form 2004 July 22

SUMMARY

Predictions of glaciation-induced changes in the Earth's rotation vector exhibit sensitivities to Earth structure that are unique within the suite of long-wavelength observables associated with glacial isostatic adjustment (henceforth GIA), and, despite nearly a quarter of a century of research, these sensitivities remain enigmatic. Previous predictions of present-day true polar wander (TPW) speed driven by GIA have indicated, for example, a strong sensitivity to variations in the thickness of the elastic lithosphere and the treatment (phase or chemical?) of the density discontinuity at 670-km depth. Nakada recently presented results that suggest that the predictions are also sensitive to the adopted rheology of the lithosphere; however, his results have introduced an intriguing paradox. In particular, predictions generated using a model with an extremely high-viscosity lithospheric lid do not converge to results for a purely elastic lithosphere of the same thickness. Mitrovica (as cited by Nakada) has suggested that the paradox originates from an inaccuracy in the traditional rotation theory (e.g. Wu & Peltier) associated with the treatment of the background equilibrium rotating form upon which any load- and rotation-induced perturbations are superimposed. We revisit these issues using a new treatment of the linearized Euler equations governing load-induced rotation perturbations on viscoelastic earth models. We demonstrate that our revised theory, in which the background form of the planet combines a hydrostatic component and an observationally inferred excess ellipticity, resolves the apparent paradox. Calculations using the revised theory indicate that earlier predictions based on earth models with purely elastic lithospheric lids are subject to large errors; indeed, previously noted sensitivities of TPW speed predictions to the thickness and rheology (elastic versus viscous) of the lithosphere largely disappear in the application of the new theory. Significant errors are also incurred by neglecting the stabilizing influence of the Earth's excess ellipticity. Finally, we demonstrate that the contribution from rotational feedback on predictions of present-day rates of change of the geoid (sea surface) and crustal velocities are overestimated by the traditional rotation theory, and this has implications for analyses of ongoing satellite (e.g. GRACE) missions and geodetic GPS surveys.

Key words: Earth rotation, glacial rebound, Liouville equations, viscoelasticity.

Downloaded from https://academic.oup.com/gji/article/161/2/491/1985141 by guest on 21 August 2022

1 INTRODUCTION

Predictions of perturbations in the Earth's rotational state driven by the glacial isostatic adjustment (GIA) process have a history that dates back a quarter of a century. Indeed, modern numerical analyses of secular changes in the orientation of the rotation vector relative to the surface geography, or true polar wander (TPW), are most commonly based on theoretical treatments described in papers by Sabadini & Peltier (1981), Yuen *et al.* (1982) and Wu & Peltier (1984). Interest in glaciation-induced rotation variations remains active, and traditional applications associated with the inference of mantle structure (e.g. Nakiboglu & Lambeck 1980; Sabadini & Peltier 1981; Yuen *et al.* 1982; Peltier & Wu 1983; Wu & Peltier 1984; Yuen & Sabadini 1985; Spada *et al.* 1992; Peltier & Jiang 1996; Vermeersen & Sabadini 1996; Vermeersen *et al.* 1997) have broadened to include studies of the feedback of rotation perturbations on a suite of other GIA observables (e.g. Han & Wahr 1989; Bills & James 1996; Milne & Mitrovica 1996, 1998; Sabadini & Vermeersen 1997; Peltier 1998; Johnston & Lambeck 1999; Mitrovica *et al.* 2001) as well as the signal from recent cryospheric forcings (e.g. Gasperini *et al.* 1986; Peltier 1988; Munk 2002).

Numerical and theoretical analyses of GIA-induced TPW have identified a suite of unique sensitivities. For example, predictions of present-day TPW speed indicate a strong sensitivity to the adopted lower mantle viscosity of the earth model (e.g. Sabadini & Peltier 1981; Yuen *et al.* 1982; Wu & Peltier 1984; Yuen & Sabadini 1985;

© 2005 RAS

Vermeersen & Sabadini 1996; Mitrovica & Milne 1998; Johnston & Lambeck 1999), to the thickness of the elastic lithosphere (e.g. Peltier & Wu 1983; Wu & Peltier 1984; Mitrovica & Milne 1998), to the treatment of the density jump at 670-km depth as some combination of phase and chemical discontinuity (e.g. Mitrovica & Milne 1998; Johnston & Lambeck 1999), and to the choice of compressible or incompressible earth model.

The highly non-monotonic sensitivity of the TPW predictions to variations in the adopted lower mantle viscosity provides an interesting contrast with other long-wavelength geophysical observables related to GIA. As the lower mantle viscosity (which we may denote by $\nu_{\rm LM}$) is increased from 10^{21} to $\sim 3 \times 10^{21}$ Pa s, numerous studies have shown that the predicted present-day TPW speed drops by $\sim$ a factor of two; as $\nu_{\rm LM}$ is increased further to 10^{22} Pa s the predicted speed oscillates about a plateau, and then once again drops monotonically as the lower mantle is progressively stiffened beyond this value. The origin of this behaviour is unclear.

In contrast, the predicted present-day secular variation in the degree-two zonal harmonic of the Earth's geopotential, $\dot{J}_2$, which is proportional to the rate of change of the Earth's axial rotation rate (e.g. Wu & Peltier 1984; Mitrovica & Milne 1998), shows a far simpler behaviour with a straightforward physical interpretation. In particular, small amplitudes are predicted for relatively weak ($\sim 10^{21}$ Pa s) and stiff ($\sim 10^{23}$ Pa s) lower mantle regions; the former because such models reach close to equilibrium $\sim$6 kyr after the end of the main glaciation phase, and the latter because such models are characterized by slow rates of adjustment throughout their evolution. The highest rates are thus predicted for intermediate values of $\nu_{\rm LM}$, leading to a double root or 'inverted parabola' structure (e.g. Ivins *et al.* 1993; Mitrovica & Peltier 1993).

The sensitivity of the TPW results becomes even more perplexing when one notes that the variation with increasing $\nu_{\rm LM}$ takes on the inverted parabola form when one considers earth models with very thin elastic lithospheres (e.g. Mitrovica & Milne 1998) or when one treats the density discontinuity at 670-km depth as a pure (adiabatic) phase boundary (e.g. Mitrovica & Milne 1998; Johnston & Lambeck 1999).

In a series of important recent papers, Nakada (2000, 2002) argued that predictions of TPW are also sensitive to the choice of rheology for the lithosphere: finite-viscosity viscoelastic or purely elastic. In this regard, Nakada (2002) pointed out an apparent paradox in his results, namely that predictions of present-day TPW speed for the case of a viscoelastic lithosphere did not converge to the predictions based on an elastic lithosphere, even when he adopted viscosities in the former as high as 10^{40} Pa s. Load-induced TPW will be sensitive to the response of the planetary model to the loading as well as to the background flattening of the model upon which the load is applied. Mitrovica (as cited by Nakada 2002) suggested that the paradox highlighted by Nakada's (2002) results may stem from an inaccuracy in the treatment of the equilibrium rotating form, and he proposed that this form should be connected to the observed flattening of the Earth. The differences in predictions based on earth models with elastic and viscoelastic lithospheres are large (Nakada 2002); indeed, the latter show a variation with $\nu_{\rm LM}$ that is akin to the inverted parabola sensitivity mapped out for predictions with no lithosphere whatsoever. Thus the discrepancy warrants further investigation.

In this paper we present a new treatment of the linearized Euler equations (i.e. the so-called Liouville equations) that govern rotation perturbations on a viscoelastic planet driven by surface loading. Our goals are to (1) isolate the origin of the paradox noted by Nakada (2002); (2) outline a revised theory that provides an accurate treatment of GIA-induced rotation perturbations on spherically symmetric earth models; and (3) explore the rotational stability inherent to the traditional and new rotation theories. Our results indicate a significant inaccuracy in the linearized rotation theory adopted over the last two decades. Furthermore, this inaccuracy is the source of much of the anomalous sensitivities evident in previous predictions of GIA-induced TPW.

2 THEORETICAL BACKGROUND AND RESULTS

2.1 The linearized Euler equations

Perturbations in the orientation of the rotation vector associated with the GIA process are small (less than $\sim 1^\circ$), and thus linearized forms of the governing Euler equations are generally adopted as a basis for the analysis. In this section we present, without detailed derivation, time- and frequency-domain forms of the so-called Liouville equations derived under the assumption that the timescale of loading is much longer than the Chandler wobble period.

In the unperturbed state (i.e. prior to loading), we adopt a body reference frame with origin at the centre of mass of the rotating planet. The orientation of this state is such that the unperturbed inertia tensor is diagonal with principal moments A, A and C, and the angular velocity vector is $\Omega = (0, 0, \Omega)$. In the perturbed state, we can write

$$w_i(t) = \Omega[\delta_{i3} + m_i(t)], \tag{1}$$

where $m_i \ll 1$ and, in addition, perturbations in the elements of the inertia tensor are $\ll A, C$.

If we introduce the complex notation $\mathbf{m}(t) = m_1(t) + i m_2(t)$, then the governing Liouville equation can, in the time domain, be written as (e.g. Nakada 2002)

$$\mathbf{m}(t) = \frac{1}{C - A}\left[\mathbf{I}^{\rm L}(t) + k_2^{\rm L}(t) * \mathbf{I}^{\rm L}(t)\right] + \frac{k_2^{\rm T}(t)}{k_{\rm f}} * \mathbf{m}(t), \tag{2}$$

where $*$ denotes time convolution. In this equation, $\mathbf{I}^{\rm L}(t)$ is the complex parameter $I_{13}^{\rm L}(t) + i I_{23}^{\rm L}(t)$, where the components are inertia tensor perturbations associated with the surface mass load redistribution (sometimes termed the inertia perturbation components for a rigid earth). Furthermore, $k_2^{\rm L}(t)$ and $k_2^{\rm T}(t)$ are the non-dimensional, degree-two, surface load and tidal viscoelastic k Love numbers, respectively. These Love numbers have the normal-mode form (Peltier 1974, 1976; Tromp & Mitrovica 1999)

$$k_2^{\rm L}(t) = k_2^{\rm L,E}\delta(t) + \sum_{k=1}^{K} r_k' e^{-s_k t}, \tag{3}$$

and

$$k_2^{\rm T}(t) = k_2^{\rm T,E}\delta(t) + \sum_{k=1}^{K} r_k'' e^{-s_{k,2} t}, \tag{4}$$

where the $\delta(t)$ is the Dirac-delta function and the superscript E denotes the elastic component. Note that the $k_2^{\rm T}$ and $k_2^{\rm L}$ Love numbers govern the gravitational potential perturbation driven by a change in the rotation vector (i.e. the adjustment of the rotational bulge) and surface mass load, respectively. Finally, the parameter $k_{\rm f}$ is the so-called fluid k Love number (Munk & MacDonald 1960), and is defined as a combination of parameters associated with the unperturbed state of the planet:

$$k_{\rm f} = \frac{3G}{a^5\Omega^2}(C - A), \tag{5}$$

where a is the radius of the Earth.

Downloaded from https://academic.oup.com/gji/article/161/2/491/1995141 by guest on 21 August 2022

Traditional GIA calculations based on spherically symmetric models commonly develop the linearized Liouville theory within the Laplace-transform domain. If we denote the transform variable as s, then the Laplace transform of eq. (2) is (e.g. Wu & Peltier 1984; Mitrovica & Milne 1998)

$$\mathbf{m}(s) = \frac{1}{C-A}\frac{\mathbf{I}^{\mathrm{L}}(s)\left[1+k_2^{\mathrm{L}}(s)\right]}{\left[1-(k_2^{\mathrm{T}}(s)/k_{\mathrm{f}})\right]}, \tag{6}$$

where the s-domain form of the viscoelastic k Love numbers is given by

$$k_2^{\mathrm{L}}(s) = k_2^{\mathrm{L,E}} + \sum_{k=1}^{K}\frac{r_k'}{s+s_k}, \tag{7}$$

and

$$k_2^{\mathrm{T}}(s) = k_2^{\mathrm{T,E}} + \sum_{k=1}^{K}\frac{r_k''}{s+s_k}. \tag{8}$$

The treatment and interpretation of the fluid k Love number, k_{f} (eq. 5), is central to discussions appearing in the remainder of this manuscript. The parameter is a measure of the background oblateness of the planet, and will in practice have contributions from the equilibrium form associated with the unperturbed rotation rate Ω (i.e. the hydrostatic form), as well as from long-term geophysical processes other than GIA (i.e. non-hydrostatic signals associated with fossil rotational effects, mantle convection, etc.) The linearized theory assumes that these contributions do not change over the course of the surface mass loading history, and that perturbations in the oblateness due to GIA are much smaller than the net background oblateness. As we will demonstrate below, approximations to k_{f} traditionally applied within the GIA literature introduce a significant error in predictions of glaciation-induced rotation perturbations. Furthermore, a recognition of this sensitivity resolves the paradox described by Nakada (2002).

2.2 k_{f}—the traditional approximation

Within the GIA literature, it has been assumed that the fluid Love number, k_{f}, can be approximated by the fluid, $s = 0$, limit of the s-domain k_2^{T} Love number (e.g. Wu & Peltier, 1984; eqs 63, 68):

$$k_{\mathrm{f}} \sim k_2^{\mathrm{T}}(s=0), \tag{9}$$

where, following eq. (8), we can write

$$k_2^{\mathrm{T}}(s=0) = k_2^{\mathrm{T,E}} + \sum_{k=1}^{K}\frac{r_k''}{s_k}. \tag{10}$$

Within the GIA literature, spherically symmetric earth models have generally been defined by the thickness of a purely elastic lithosphere and a radial profile of mantle viscosity. The parameter $k_2^{\mathrm{T}}(s=0)$ is independent of the latter; however, it is a function of the background density profile and the thickness of the elastic lithosphere (denoted as 'LT'). Henceforth, we will commonly adopt a notation, $k_2^{\mathrm{T}}(s=0;LT)$, which makes this latter dependence explicit.

Using the approximation (9), the governing Liouville equations (2) and (6) become

$$\mathbf{m}(t) = \frac{1}{C-A}\left[\mathbf{I}^{\mathrm{L}}(t) + k_2^{\mathrm{L}}(t) * \mathbf{I}^{\mathrm{L}}(t)\right] + \frac{k_2^{\mathrm{T}}(t)}{k_2^{\mathrm{T}}(s=0;LT)} * \mathbf{m}(t) \tag{11}$$

and

$$\mathbf{m}(s) = \frac{1}{C-A}\frac{\mathbf{I}^{\mathrm{L}}(s)\left[1+k_2^{\mathrm{L}}(s)\right]}{\left[1-k_2^{\mathrm{T}}(s)/k_2^{\mathrm{T}}(s=0;LT)\right]}, \tag{12}$$

where LT in $k_2^{\mathrm{T}}(s=0;LT)$ refers to the elastic lithospheric thickness adopted to compute the time- and s-domain Love numbers $k_2^{\mathrm{T}}(s)$, $k_2^{\mathrm{T}}(t)$, $k_2^{\mathrm{L}}(s)$, and $k_2^{\mathrm{L}}(t)$. Wu & Peltier (1984) have provided analytic expressions for the inverse Laplace transform applied to eq. (12). Their result, which involves a set of so-called 'rotational normal modes', is summarized in Appendix A.

Why have previous analyses adopted the approximation (9) for the fluid Love number k_{f}? The k_2^{T} Love number can be used to approximate (to the accuracy of the perturbation theory upon which this number is based) the equilibrium form of a rotating planet (Munk & MacDonald 1960). Consider a model earth with an elastic shell of thickness LT that is set spinning at the current rotation rate of Ω. The equilibrium rotating form of this planet can be related to the fluid limit of the k_2^{T} Love number computed for this model by (e.g. Mound *et al.* 2003)

$$k_2^{\mathrm{T}}(s=0;LT) = \frac{3G}{a^5\Omega^2}(C-A)_{LT}, \tag{13}$$

where $(C-A)_{LT}$ is the *predicted* difference in the polar and equatorial moments of inertia for this model rotating earth with elastic shell thickness LT . In Fig. 1 we show a prediction of $k_2^{\mathrm{T}}(s=0;LT)$ as a function of LT computed using the seismic density model PREM (Dziewonski & Anderson 1981). As one would expect, increasing the thickness of the elastic shell acts to reduce the rotationally induced oblateness of the earth model (see also Mound *et al.* 2003). The arrows on Fig. 1 specify the observed value of k_{f} (i.e. eq. 5 with observed quantities applied) and a prediction by Nakiboglu (1982) based on second-order-accurate hydrostatic ($LT = 0$) theory.

A comparison of eq. (13) with the correct expression (5), where the latter involves the initial (or unperturbed) difference $C - A$, makes clear the set of approximations inherent to the traditional assumption (9). The following assumptions have previously been made. (1) The difference in the polar and mean equatorial moments of inertia of the planet is governed entirely by the equilibrium rotating form of the planet associated with the present rotation rate. Thus, other geophysical processes contributing to this form, for example convection-induced dynamic ellipticity or a fossil rotational

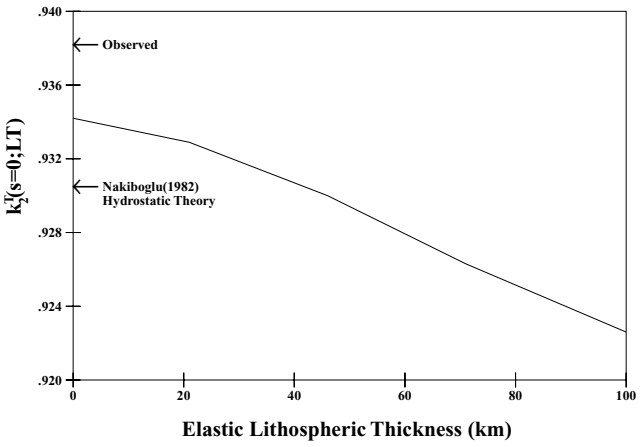

Figure 1. The solid line shows numerical predictions of the degree-two tidal Love number in the $s = 0$ fluid limit, $k_2^{\mathrm{T}}(s=0;LT)$, as a function of the thickness of the purely elastic lithosphere (LT) adopted in the earth model. The radial profile of density is given by PREM (Dziewonski & Anderson 1981). The arrow at top left provides the 'observed' fluid Love number, as defined by eq. (5), where present-day values of Ω, C and A are adopted (as in eq. 14). The second arrow shows the fluid Love number computed for PREM by Nakiboglu (1982) using a second-order-accurate hydrostatic ($LT = 0$) theory.

Downloaded from https://academic.oup.com/gji/article/161/2/491/1995141 by guest on 21 August 2022

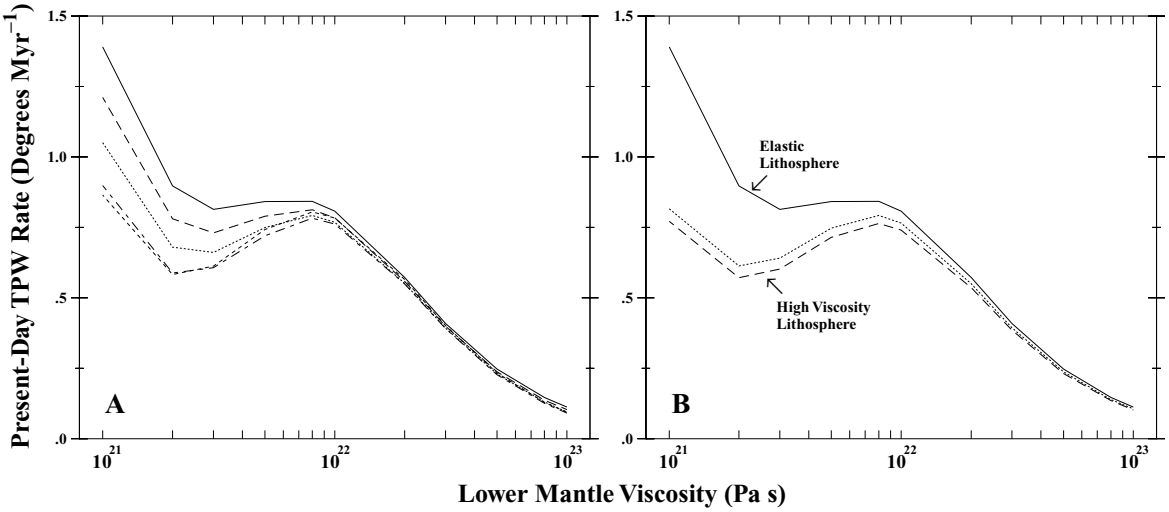

Figure 2. Predictions of present true polar wander speed, as a function of the lower mantle viscosity (abscissa scale) of the earth model, generated using the traditional treatment of k_f as $k_2^T(s = 0; LT)$ (eq. 9). The predictions are performed using the time-domain form of the governing equations (see eq. 11). (a) A sequence of predictions distinguished on the basis of the adopted thickness of a purely elastic lithosphere: $LT = 100$ km (solid line), 71 km (dashed line), 46 km (dotted line), 21 km (dashed–dotted line) and 0 km (short-dashed line). (b) Solid line is identical to the results in (a) (i.e. LT= 100 km); in contrast, the remaining two lines are generated using no purely elastic lithosphere ($LT = 0$ km), but viscosities in the top 100 km of the model are set to either 10^{24} Pa s (dashed line) or 10^{28} Pa s (dotted line). In all predictions in the figure the upper mantle viscosity (below the elastic lithosphere on the left frame and below 100 km depth on the right frame) is set to 10^{21} Pa s. The surface mass load history is described in the text.

bulge, are neglected. (2) This equilibrium form can be computed with sufficient accuracy using viscoelastic Love number theory applied to the *same* earth model as used to compute the response of the earth to the surface loading and rotation perturbations. That is, as we have discussed, the earth model used to compute the time- and s-domain Love numbers $k_2^T(s)$, $k_2^T(t)$, $k_2^L(s)$, and $k_2^L(t)$ in the Liouville equations is the same model as used to compute the background equilibrium form.

The dependence of the prediction of $k_2^T(s = 0; LT)$ on the underlying earth model (and specifically on the adopted elastic lithospheric thickness) appears to be relatively modest, but nevertheless this dependence lies at the heart of the paradox discovered by Nakada (2002). A prediction of glaciation-induced polar wander is dependent both on the manner in which the model planet responds to the applied surface mass and rotational loading, and on the background (or unperturbed) oblateness of the planet. In the generalized theory (eqs 2–6) the latter is given by k_f; the approximation (9) introduces an erroneous model (i.e. LT) dependence in this background form.

The paradox Nakada (2002) discovered was as follows. His predictions of present-day TPW speed computed using a purely elastic lithosphere were different from predictions based on a viscoelastic lithosphere of the same thickness even when the viscosity of the latter lithosphere was set to an extremely high value (10^{40} Pa s). How could this be? Given the short timescale of GIA relative to the extremely long Maxwell time of a lithosphere of viscosity 10^{40} Pa s, these two models (high-viscosity viscoelastic, and elastic) would certainly respond with the same deformation if subject to an identical applied surface mass load or rotational driving potential. However, by making the assumption (9), as all previous studies had done, Nakada (2002) was introducing a difference in the background oblateness of the two models. Specifically, $k_2^T(s = 0)$ for a model with an extremely high- (but still finite) viscosity, 100-km-thick lithosphere is identical to $k_2^T(s = 0)$ for a model with no elastic lithosphere (the left-hand intercept of the curve in Fig. 1; i.e. $LT = 0$ in both cases); in contrast, $k_2^T(s = 0)$ for a model with an elastic lithosphere of 100-km thickness ($LT = 100$ km) is given by the right intercept in Fig. 1. By adopting $k_2^T(s = 0)$ as an approximation for k_f, the two models were implicitly given distinct initial background forms, and thus the computed TPW for the two cases should not necessarily converge.

Despite the apparently modest dependence of $k_2^T(s = 0; LT)$ on the thickness of the elastic lithosphere (Fig. 1), Nakada's (2002) results indicate that the impact of the approximation to k_f on predictions of TPW can be significant. In Fig. 2 we present a suite of predictions of present-day TPW speed which reproduce these general results. In these, and all subsequent predictions, we consider a simplified model of the late Pleistocene ice-load history introduced by Mitrovica & Milne (1998) (and adopted by Nakada 2002). Specifically, we include a series of eight 100-kyr glacial cycles, with each cycle defined by a 90-kyr glaciation phase and a 10-kyr deglaciation period. This sawtooth time history is characterized by inertia perturbations of $I_{13}^L = -6.67 \times 10^{31}$ kg m^2, $I_{23}^L = 2.31 \times 10^{32}$ kg m^2, and $I_{33}^L = -7.89 \times 10^{31}$ kg m^2, at each glacial maximum. These values are estimated from a global reconstruction of ice volume at last glacial maximum (Tushingham & Peltier 1991) and a complementary eustatic ocean load (Mitrovica & Milne 1998). The last glacial cycle is assumed to end 6 kyr before present. The predictions shown in the figure are based on the time-domain Liouville equation (11), although we have confirmed that predictions based on eq. (12) yield the same results.

Fig. 2(a) shows results for a sequence of values of the thickness of the elastic lithosphere, LT, ranging from 100 km (solid line) to 0 km (short-dashed line) as a function of the adopted lower mantle viscosity (ν_{LM}). This sequence of results shows the dependence on the thickness of the elastic lithosphere observed in numerous previous studies. In Fig. 2(b) the results for $LT = 100$ km are reproduced, together with predictions based on a 100-km viscoelastic lithosphere with a viscosity of either 10^{24} Pa s (dashed line) or 10^{28} Pa s (dotted line). The discrepancy between the solid and dotted lines in Fig. 2(b) is an illustration of the Nakada (2002)'paradox'.

Downloaded from https://academic.oup.com/gji/article/161/2/491/1995141 by guest on 21 August 2022

As we have discussed, each choice of the thickness of the elastic lithosphere, LT, in Fig. 2 yields a different value for $k_2^{\rm T}(s = 0; LT)$ (Fig. 1) and thus a different approximation (via eq. 9) to the fluid Love number $k_{\rm f}$ (and background planetary oblateness). As an example, in Fig. 2(b), the solid line joins results for models with $k_2^{\rm T}(s = 0; LT = 100) \sim 0.922$, while the remaining lines are constructed from models with $k_2^{\rm T}(s = 0; LT = 0) \sim 0.934$ (Fig. 1)—a difference of 1.5 per cent. The discrepancy between the solid and dotted lines in Fig. 2(b) indicates that predictions of GIA-induced present-day TPW speed are progressively more sensitive to variations in the adopted (LT-dependent) background planetary oblateness as the lower mantle viscosity is reduced. Indeed, the sensitivity of the predictions to the 1.5 per cent variation cited above is, for $\nu_{\rm LM} \sim 10^{21}$ Pa s, remarkably large (see also Nakada 2002).

The form of the governing equations suggests that some form of instability may be at play. In particular, note that the s-domain Liouville equation, when $k_{\rm f}$ is approximated by $k_2^{\rm T}(s = 0; LT)$ (12), becomes unstable in the fluid ($s = 0$) limit since the denominator will approach zero in this limit. This is a restatement of the well-known result that the orientation of a rotating body in hydrostatic equilibrium is unstable in the presence of uncompensated surface mass changes (Goldreich & Toomre 1969). We explore the issue of stability in detail in Figs 3 and 4.

Fig. 3 shows a decomposition of the model-dependent components of the governing equation (12) as a function of the Laplace transform variable s. Each frame shows results for four earth models distinguished on the basis of the lower mantle viscosity: 10^{21} Pa s (solid line), 3×10^{21} Pa s (dashed line), 10^{22} Pa s (dotted line) and 3×10^{22} Pa s (dashed–dotted line). In all cases $LT = 100$ km. Fig. 3(a) gives $1 - k_2^{\rm T}(s)/k_2^{\rm T}(s = 0; LT = 100)$, i.e. the denominator in eq. (12), which is a measure of the s (or frequency) dependence in the adjustment of the rotational bulge (a value of 0 reflects complete adjustment of the bulge to a perturbation in rotation). Fig. 3(b) shows $1 + k_2^{\rm L}(s)$, i.e. the numerator of the model-dependent term of eq. (12), which is an s-dependent measure of the compensation of the surface mass load. Fig. 3(c) provides the ratio of these two dependences over a slightly smaller range of s values. The right (high s, short timescale) intercept represents the elastic limit, while the left (small s, long timescale) intercept is the fluid limit. The four models have the same elastic asymptotes, since we adopt PREM in all cases, and $s = 0$ fluid asymptotes, since $LT = 100$ in all cases; thus, the asymptotic trends in Figs 3(a) and (b) converge. Not surprisingly, for a given s value, models with progressively weaker lower mantle viscosity are closer to the fluid limit associated with the response to both the surface mass and rotational forcing.

The results in Fig. 3(c), as s approaches the fluid limit, reflect the instability described above. In particular, for small s, the isostatic compensation of the surface load is less complete than the adjustment of the rotational bulge (i.e. the denominator, as shown in Fig. 3(a), converges to 0 at small s, whereas the numerator, as shown in Fig. 3(b), does not), and the result is a ratio that exhibits a rapid increase in amplitude. As the lower mantle viscosity is weakened, the instability initiates at larger values of s (smaller timescales), and the amplitude of the predicted present-day TPW speed (solid line, Fig. 2a) reflects this trend.

In Fig. 4 we repeat the analysis of Fig. 3 for three models with the same lower mantle viscosity (10^{21} Pa s) but distinct treatments of the lithosphere. The solid line is based on a model with an elastic lithosphere of thickness 100 km (these are identical to the solid lines in Fig. 3). In contrast, the remaining two lines adopt $LT = 0$ and are distinguished on the basis of the viscosity within the top 100 km: either 10^{21} Pa s (i.e. the same as the remaining upper mantle; dashed–dotted lines) or 10^{28} Pa s (i.e. a high-viscosity—but not elastic—lid; dotted lines). The results in Fig. 4(c) indicate that the latter two models both exhibit a more stable rotational state for small s values (less than ∼0 on the abscissa, or timescales greater than 1000 yr) than the $LT = 100$-km prediction. As we will discuss, the origin of this increased stability is different for the two cases.

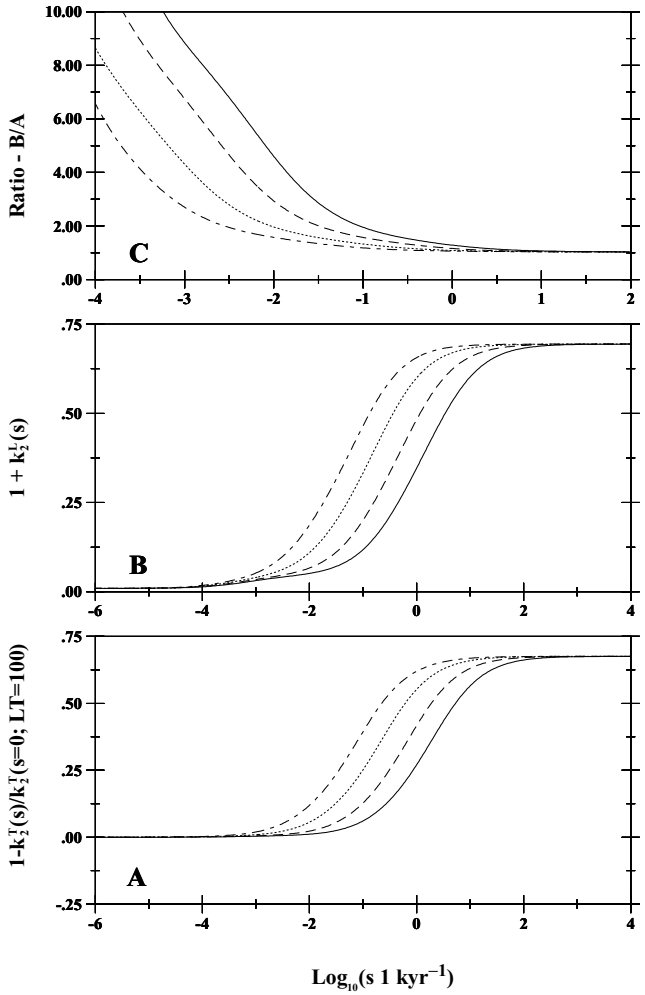

Figure 3. Decomposition of the model-dependent components of the traditional Liouville equation (12) as a function of the Laplace transform variable s: (a) $1 - k_2^{\rm T}(s)/k_2^{\rm T}(s = 0; LT)$; (b) $1 + k_2^{\rm L}(s)$; and (c) the ratio (b/a) of these terms. In each frame, results are shown for four earth models with distinct $\nu_{\rm LM}$: 10^{21} Pa s (solid line); 3×10^{21} Pa s (dashed line); 10^{22} Pa s (dotted line); and 3×10^{22} Pa s (dashed–dotted line). In each case, $LT = 100$ km and the upper mantle viscosity is 10^{21} Pa s.

We begin by comparing the solid and dashed–dotted lines. In this case, the models are identical in all respects with the exception that the lithospheric thickness is reduced from 100 km to 0. The models have the same elastic Love numbers, but for any s other than the elastic limit (including the fluid, $s = 0$ limit) the Love numbers will differ because of the distinct values of the adopted LT. The solid and dashed–dotted lines are nearly indistinguishable in Fig. 4(a), indicating that a simple reduction in the lithospheric thickness (from 100 km to 0) makes negligible difference to the adjustment of the rotational bulge over timescales relevant to GIA. In contrast, this reduction clearly impacts the level of isostatic compensation of the surface mass load (Fig. 4b). As LT is reduced, while maintaining a constant sublithospheric upper mantle viscosity, the term $1 + k_2^{\rm L}(s)$

Downloaded from https://academic.oup.com/gji/article/161/2/491/1995141 by guest on 21 August 2022

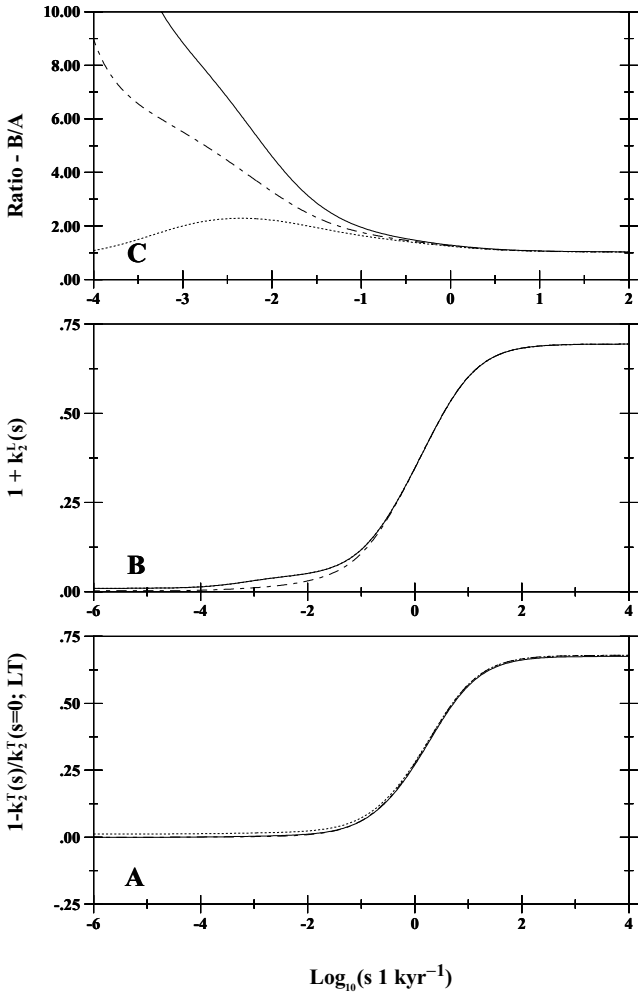

Figure 4. As in Fig. 3, except for a set of three earth models distinguished on the basis of our treatment of the lithosphere. In all cases both $\nu_{\rm LM}$ and the upper mantle viscosity (below the lithosphere) are 10^{21} Pa s. Solid line: an elastic lithosphere of thickness $LT = 100$ km (same as solid line in Fig. 3); dashed–dotted line: $LT = 0$ and the viscosity of the top 100 km of the model is set to the upper mantle viscosity; dotted line: $LT = 0$ and the top 100 km of the model is given a high-viscosity (10^{28} Pa s) lithospheric lid.

in eq. (12) more closely approaches zero (i.e. perfect compensation) and the rotation pole is stabilized. This explains the reduction in amplitude of the predicted TPW speed in Fig. 2(a) as LT is reduced.

Finally, consider the solid and dotted lines in Fig. 4. These lines are indistinguishable in Fig. 4(b). As we described earlier, this simply indicates that the isostatic compensation of the surface mass load over these timescales will be the same for a model with an elastic lithosphere and a model with a very high-viscosity lithosphere of the same thickness (i.e. over the s range in Fig. 4(b), $k_2^{\rm L}(s)$ is the same for both models). However, a difference between the two model predictions is evident in Fig. 4(a). In this case, the Love number $k_2^{\rm T}(s)$ is also essentially identical for the two models over the range of s values on the figure; however, the adopted value of $k_2^{\rm T}(s = 0; LT)$ (i.e. the background oblateness) will be different in the two cases. For such a high-viscosity lid, s values will have to be significantly smaller (timescales significantly larger) than those shown on the figure before the lid viscously relaxes and $k_2^{\rm T}(s)$ obtains its fluid limit; thus, the term $1 - k_2^{\rm T}(s)/k_2^{\rm T}(s = 0; LT = 0)$ for the high-viscosity-lid case (dotted line) is shifted away from 0.0 relative to the $1 - k_2^{\rm T}(s)/k_2^{\rm T}(s = 0; LT = 100)$ case and the rotation is stabilized (Fig. 4c). The small deviation in Fig. 4(a) is thus responsible for the large difference in the predicted TPW speeds (solid, dotted lines) in Fig. 2(b) and the paradox described by Nakada (2002).

The relative accuracy of the TPW rate predictions in Fig. 2 is not clear since the relation between the value of $k_2^{\rm T}(s = 0; LT)$ adopted in eq. (11) and the appropriate value for $k_{\rm f}$ is unclear. This issue is addressed in the next section, where we present predictions based on an improved expression for $k_{\rm f}$.

2.3 $k_{\rm f}$—a new approach

The parameter $k_{\rm f}$ in the generalized Liouville equations (2) and (6) represents, via eq. (5), a measure of the background oblateness of the planet upon which the Late Pleistocene glaciation cycles have been superimposed. The linearization procedure used to derive these equations assumes that perturbations in $k_{\rm f}$ (i.e. oblateness) due to GIA, or any other time-dependent geophysical process for that matter, have been small since the onset of ice-age loading (several million years ago). In this case, following the suggestion by Mitrovica (see Nakada 2002), a logical approach to the rotation problem would be to solve the generalized Liouville equations with $k_{\rm f}$ replaced by the observed (present-day) value of this parameter (which we will denote by $k_{\rm f}^{\rm obs}$). That is, one can use

$$k_{\rm f} \sim k_{\rm f}^{\rm obs} = \frac{3G}{a^5\Omega^2}(C - A)_{\rm obs} \sim 0.9382 \qquad (14)$$

in eqs (2) and (6), where $(C - A)_{\rm obs}$ is the *observed* difference in the polar and equatorial moments of inertia. The observed fluid Love number is shown superimposed on Fig. 1. We have found, using results from our suite of numerical predictions of the GIA process, that the perturbation in $k_{\rm f}$ associated with GIA (which is proportional to the perturbation in the J_2 harmonic of the geopotential) is less than $\sim$0.001. This supports the validity of the linearization procedure, as well as Mitrovica's suggestion that eq. (14) be adopted in the Liouville equations. The expression (14), in contrast to the traditional approximation (9), clearly introduces no model dependence in the background oblateness.

As is clear from the discussion of the last section, the stability of the rotation axis in the presence of an applied surface mass load is intimately connected to the expression $1 - k_2^{\rm T}(s)/k_{\rm f}$ appearing in the denominator of the Liouville equation (6). From Fig. 1, the observed fluid Love number, $k_{\rm f}^{\rm obs}$, is greater than $k_2^{\rm T}(s = 0; LT)$ for any value of LT (we comment on the origin of this difference below); thus, adopting the expression (14) will, in addition to improving the accuracy of the predictions, stabilize the rotation axis relative to predictions based on the approximation (9).

If one adopts the observed fluid Love number in place of $k_{\rm f}$, then the accuracy of the predictions may still be impacted by errors in the viscoelastic Love number theory used to generate $k_2^{\rm T}(s)$ (that is, by errors incurred by ignoring second and higher-order terms in the first-order Love number theory). To highlight this point, we also superimpose on Fig. 1 the value of $k_2^{\rm T}(s = 0; LT = 0)$ computed by Nakiboglu (1982) using his second-order-accurate hydrostatic theory applied to PREM. The difference between this value (0.9305) and the left intercept of the solid line, which represents the hydrostatic form predicted using Love number theory, provides a measure of the accuracy of the latter. This error, interestingly a 1 part in 300 overestimate, would have implications for the predicted stability of the rotation axis. In particular, the expression $1 - k_2^{\rm T}(s)/k_{\rm f}^{\rm obs}$, where $k_2^{\rm T}(s)$ is based on viscoelastic Love number theory, will approach

Downloaded from https://academic.oup.com/gji/article/161/2/491/1995141 by guest on 21 August 2022

zero more closely than would a second-order-accurate theory; thus, predictions based on this theory will still underestimate the true stability of the rotation pole, even when k_f has been appropriately replaced by the observed value, as in eq. (14).

In the remainder of this section we propose two conceptually independent, but ultimately equivalent, approaches to further improving the accuracy of TPW predictions beyond the level obtainable with the combined eqs (6) and (14).

Nakada (2002) suggested that one possible route to avoiding the paradox in his results (for a very high-viscosity lithosphere and an elastic lithosphere of equal thickness; Fig. 2b) was to use the approximation

$$k_f \sim k_2^T(s = 0; LT = 0) \tag{15}$$

in the Liouville equations. That is, he suggested that, regardless of the model used to predict the deformational response to the surface mass load and rotation perturbation, one adopt the fluid limit of the $k_2^T(s)$ Love number computed for a model with no elastic lithosphere ($LT = 0$) as a proxy for the fluid Love number in the Liouville equations (2) or (6). (In Fig. 1, k_2^T ($s = 0$; $LT = 0$) = 0.934.)

While this suggestion might seem ad-hoc, there is some reasonable justification for considering it. In particular, in the absence of other geophysical contributors (e.g. plate tectonics) or a fossil rotational bulge, the equilibrium rotating form of the Earth would be most accurately computed for models with no purely elastic strength in the lithosphere (i.e. pure hydrostatic theory); note, in this regard, that $k_2^T(s = 0; LT)$ tends toward k_f^{obs} in Fig. 1 as LT approaches zero. This hydrostatic rotational form would be set early in Earth history, when $LT \sim 0$, and any subsequent increase in elastic strength would develop on this pre-existing form. That is, a slowly developing elastic strength of the lithosphere as the planet cools would exert no elastic stresses on this pre-existing form; however, the elastic strength would be important, and should be included (as it generally is), when considering any recent response of the planet to a surface mass or rotational load. (As a small digression, Mound *et al.* (2003) have recently considered the equilibrium form of a rotating planet with a thin elastic shell. Although the theory they describe is correct, it has limited relevance to understanding the present-day oblateness of the Earth; the usual hydrostatic theory with $LT = 0$ is more appropriate.) Thus, LT might be set to zero when considering the background oblateness, but LT should not be zero when treating the Pleistocene deformational response of the planet to a surface mass or rotational loading.

Of course, the primary problem with the approximation (15) is that it ignores other geophysical contributions to the background oblateness of the planet. In reference to Fig. 1, the difference between the observed fluid Love number and that obtained by second-order hydrostatic theory (0.938–0.9305 $\sim$ 0.008) represents an excess ellipticity (henceforth β) of the planet that is widely interpreted as being dynamically supported by mantle convective flow. A more accurate prediction of the rotational response of the planet would be obtained by revising the approximation (15) to include this excess ellipticity:

$$k_f \sim k_2^T(s = 0; LT = 0) + \beta = 0.942 \tag{16}$$

(where $\beta = 0.008$). When this equation is applied to the s-domain Liouville equation (6), the denominator of the model-dependent term becomes $1 - k_2^T(s)/[k_2^T(s = 0; LT = 0) + 0.008]$; this expression clearly includes the stabilizing influence of the Earth's inferred excess ellipticity, while having the advantage of involving terms ($k_2^T(s)$, $k_2^T(s = 0; LT = 0)$) that are computed using a consistent (Love number, first-order) level of accuracy.

As a second approach, we begin with the expression (14). In contrast to the approximation (9) or (15), adopting the observed fluid Love number in place of k_f in the Liouville theory implicitly incorporates all processes contributing to the background form (e.g. mantle convection, etc.). However, when eq. (14) is combined with the s-domain Liouville equation (6), the denominator of the governing equation becomes $1 - k_2^T(s)/k_2^{obs}$, and, as we discussed above, the accuracy of this expression is impacted by errors in the first-order-accurate viscoelastic Love number theory used to compute $k_2^T(s)$. The difference between the hydrostatic ($LT = 0$) predictions based on viscoelastic Love number theory and Nakiboglu's (1982) second-order approach (see Fig. 1) suggests a fractional error in the former of $\epsilon = (0.934–0.9305)/0.9305 \sim 0.0037$. Assuming that this error holds for all s values, and not simply the hydrostatic ($s = 0$) case, we can scale $k_2^T(s)$ computed using viscoelastic Love number theory by a factor $(1 - \epsilon)$ to correct for the error in the first-order theory. In this case, the denominator in the governing s-domain equation would become $1 - k_2^T(s)(1 - \epsilon)/k_2^{obs}$. Since $\epsilon \ll 1$, this is equivalent to revising eq. (14) for k_f to

$$k_f \sim k_f^{obs}(1 + \epsilon) = 0.942. \tag{17}$$

While we have used conceptually different approaches to derive eqs (16) and (17), the final expressions for k_f are identical.

The traditional approach to computing GIA-induced perturbations in the Earth's rotation vector (eqs 11 and 12) should be replaced by a combination of the general Liouville equations (2 and 6) and the expression (16) or (17) for the fluid Love number k_f. The new theory avoids the erroneous, model-dependent treatment of the background form that is inherent to the traditional theory, while incorporating the stabilizing influence on the rotation axis of the excess (i.e. non-hydrostatic) bulge of the planet.

In Fig. 5 we show predictions of present-day TPW speed generated using the new theory for the set of earth models adopted in Fig. 2. A comparison of Figs 2 and 5 indicates profound differences. The results in Fig. 5(a) show that predictions of present-day TPW speed due to GIA are, in contrast to conclusions based on the traditional rotation theory, insensitive to variations in the adopted thickness of the elastic lithosphere. In reference to remarks in the Introduction, we also conclude that the unique sensitivities evident in previous predictions of present-day TPW speed (e.g. Fig. 2a), relative to other long-wavelength observables associated with GIA (e.g. $\dot{J}_2$), are a result of the error introduced by the approximation (9) for the background form of the planet.

Fig. 5(b) shows results for predictions with $LT = 100$ km (solid line) and a pair of earth models with a viscoelastic lithosphere of increasing viscosity. The very high-viscosity (10^{28} Pa s) lithosphere results (dotted line; not evident below the solid) have converged to the $LT = 100$-km suite of predictions. Our revised theory ensures that *both* the deformational response to surface mass and rotational loading associated with GIA *and* the background form (oblateness) of the planet are identical for models with a high-viscosity lithosphere and an elastic lithosphere of equal thickness. The 'paradox' introduced by the previous approximation (9) thus disappears.

The stabilizing influence of using eqs (16) or (17) in place of the traditional approximation (9) is explored in detail in Figs 6 and 7, where we consider a decomposition of the model-dependent terms in the s-domain Liouville equation (6): (a) $1 - k_2^T(s)/k_f$, (b) $1 + k_2^L(s)$, and (c) their ratio. These figures may be directly compared with analogous plots for the traditional TPW theory, Figs 3 and 4, respectively. Since the only difference between the old and new approaches is in the treatment of k_f, Figs 3(b) and 6(b), as well as Figs 4(b) and 7(b), are identical.

Downloaded from https://academic.oup.com/gji/article/161/2/491/1995141 by guest on 21 August 2022

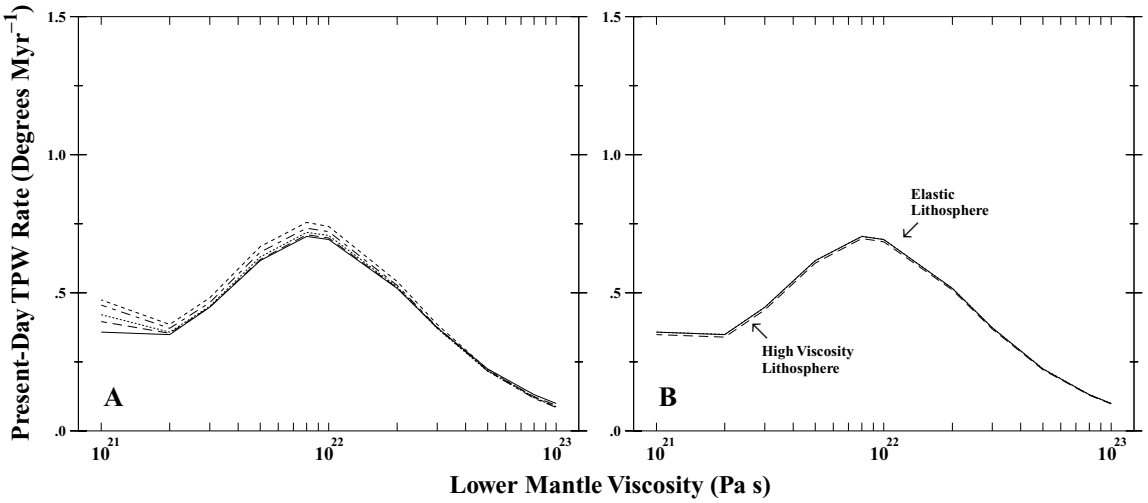

Figure 5. As in Fig. 2, except the predictions are generated using the generalized time-domain Liouville equations (2; with k_f given by eq. 16) (or eq. 17). Note that the dotted line in the right frame is indistinguishable from the solid line.

Fig. 6 shows results for a suite of models with different lower mantle viscosities and $LT = 100$. Following eq. (16), $k_f = 0.942$ as opposed to $k_f = k_2^T(s = 0; LT = 100) \sim 0.923$ (Fig. 1), the value adopted using the traditional theory. As a consequence, the denominator $1 - k_2^T(s)/k_f$ is shifted away from zero in Fig. 6(a) relative to Fig. 3(a), and the result is a dramatic stabilization of the rotational state (compare Figs 3c and 6c). Fig. 7 involves three models, all with $\nu_{LM} = 10^{21}$ Pa s. The solid line is the case for $LT = 100$, while the dotted line (which is indistinguishable from the solid) was computed using a high-viscosity (10^{28} Pa s) lid of the same thickness but with $LT = 0$. Since the s-domain Love numbers $k_2^T(s)$ and $k_2^L(s)$ for these two models are the same over the s range considered in the plot, and since the new theory removes any model (LT) dependence in k_f, no difference is seen between the two predictions of the rotational state and its contributions; thus, the paradox observed by Nakada (2002) is reconciled (as in Fig. 5b). The dashed–dotted line in Fig. 7 is a prediction for $LT = 0$ and no lithospheric lid; in this case, the earth model shows higher levels of compensation in response to the rotational forcing on the bulge (a) and the surface mass load (b), relative to the $LT = 100$ case, and the net effect is a ratio (c) reflecting comparable rotational stability for the two cases ($LT = 0$, 100 km). Hence, predictions of present-day TPW speed based on the new theory are relatively insensitive to variations in LT (Fig. 5a).

To this point we have focused entirely on predictions of present-day TPW speed. In Fig. 8 we compare predictions of the pole displacement, relative to the present value (hence all curves pass through zero at present), over roughly the last ~90 kyr. These predictions were computed using models with a thickness of the elastic lithosphere of 100 km, and two values of lower mantle viscosity (as labelled by 'LM' on each frame). Furthermore, in each case we solved the time-domain Liouville equation (2), with the fluid Love number k_f given either by the traditional approximation (9; solid line), or the new approach (16, 17; dashed line). Fig. 9 shows analogous results, except for the variation in TPW speed over the same period.

In both figures it is clear that the traditional approximation adopted in the GIA literature, that the background oblateness in the Liouville equations can be specified using $k_2^T(s = 0; LT)$, yields predictions of the pole path that are significantly discrepant from predictions where the oblateness is a model-independent reflection

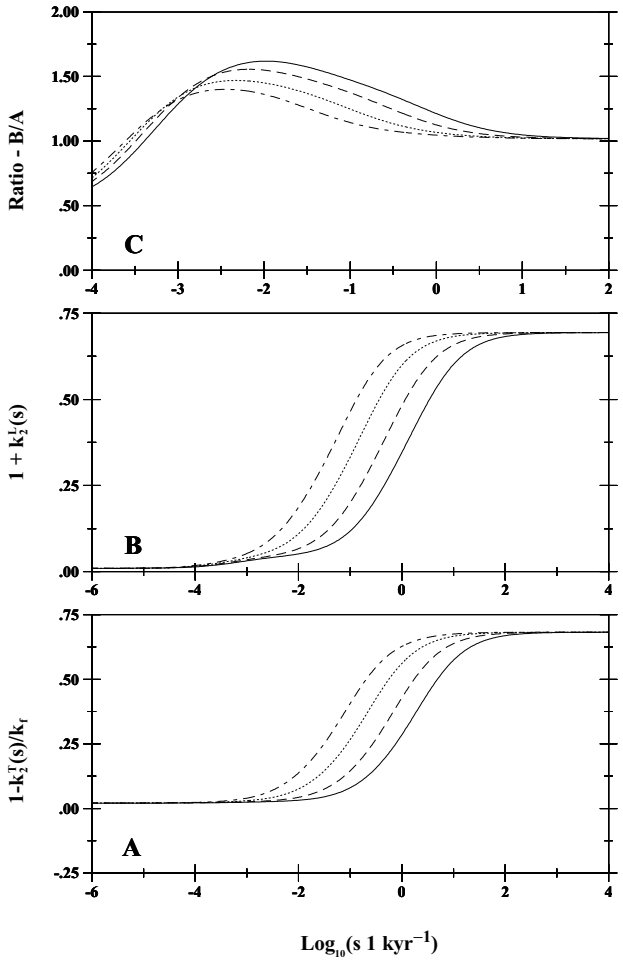

Figure 6. Decomposition of the model-dependent components of the generalized Liouville equation (6) as a function of the Laplace transform variable s: (a) $1 - k_2^T(s)/k_f$, where k_f is given by eq. (16) or (17); (b) $1 + k_2^L(s)$; and (c) the ratio (b/a) of these terms. In each frame, results are shown for four earth models with distinct ν_{LM} : 10^{21} Pa s (solid line); 3×10^{21} Pa s (dashed line); 10^{22} Pa s (dotted line); and 3×10^{22} Pa s (dashed–dotted line). In each case, $LT = 100$ km and the upper mantle viscosity is 10^{21} Pa s. Note that part (b) is identical to Fig. 3(b).

Downloaded from https://academic.oup.com/gji/article/161/2/491/1995141 by guest on 21 August 2022

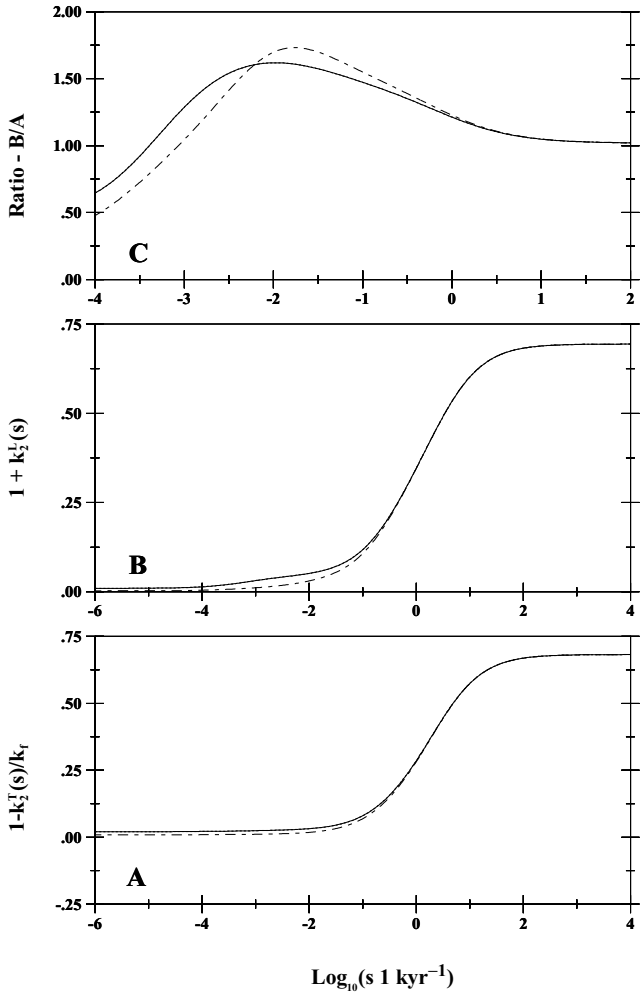

Figure 7. As in Fig. 6, except for a set of three earth models distinguished on the basis of our treatment of the lithosphere. In all cases both $\nu_{\rm LM}$ and the upper mantle viscosity (below the lithosphere) are 10^{21} Pa s. Solid line: an elastic lithosphere of thickness $LT = 100$ km (same as solid line in Fig. 6); dashed–dotted line: $LT = 0$ and the top 100 km of the model is set to the bulk upper mantle viscosity; dotted line: $LT = 0$ and the top 100 km of the model is given a high-viscosity (10^{28} Pa s) lithospheric lid. The dotted line is indistinguishable from the solid line in all frames. Note that part (b) is identical to Fig. 4(b).

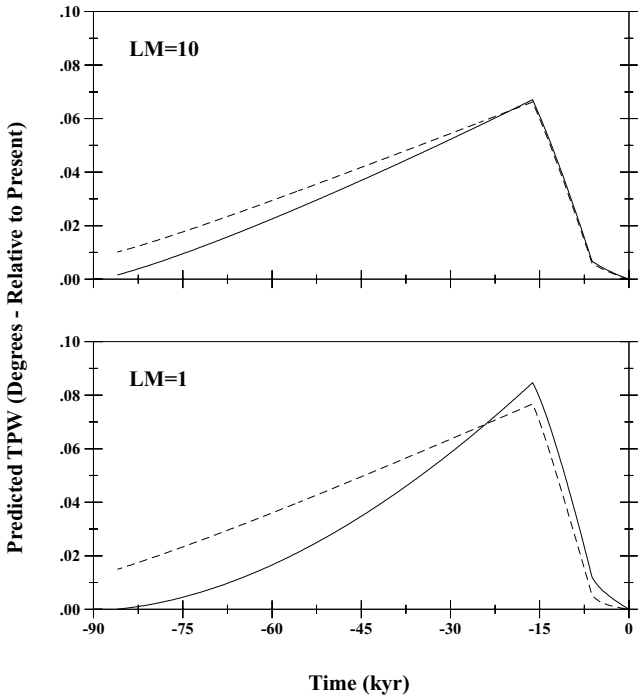

Figure 8. Predictions of the displacement of the rotation pole over the last ∼90 kyr of the loading history, relative to the present position, computed using an earth model with a purely elastic lithosphere of thickness 100 km, an upper mantle viscosity of 10^{21} Pa s, and a lower mantle viscosity of either 10^{21} Pa s (bottom frame) or 10^{22} Pa s (top frame). In each frame the solid line was generated using a time-domain form of the governing Liouville equation with $k_{\rm f}$ given by the traditional approximation (9) (i.e. $k_{\rm f} = k_2^{\rm T}(s = 0; LT)$). The dashed line uses our new formulation (eqs 16 or 17) for the fluid Love number. The surface mass loading is described, in detail, in the text.

of the hydrostatic form plus excess ellipticity. As one would expect from Figs 2 and 5, the predicted discrepancy is smaller for the model with the higher lower mantle viscosity of 10^{22} Pa s. We also note, in reference to Fig. 9, that the discrepancy in the predicted present-day TPW speed between Figs 2 and 5 is established by the end of the deglaciation event, at 6 kyr before present; that is, the absolute change in the predicted TPW speed over the last 6 kyr is largely the same in the two formulations.

The derivation of our new expressions for the fluid Love number $k_{\rm f}$ assumes a value of $\beta = 0.008$ for the contribution associated with the excess (i.e. non-hydrostatic) ellipticity of the planet; this assumption is explicit in eq. (16) and implicit in eq. (17). This value of β is inferred from the difference between the observed $k_{\rm f}$ and the fluid Love number predicted by Nakiboglu (1982) using a second-order-accurate hydrostatic theory (Fig. 1). Since the latter depends on the density model (Nakiboglu used the PREM density profile), the inference of β is subject to uncertainty. To explore this issue we repeated the $LT = 100$ calculations shown in Fig. 5(a) (solid line, $\beta = 0.008$) for a suite of choices for the β parameter in eq. (16). The results are shown in Fig. 10.

Not surprisingly, as the β value is increased from 0.0 to 0.010, the stability of the rotation pole increases and the amplitude of the predicted TPW speed monotonically falls. In the $\beta = 0$ case, the general expression (16) reduces to the approach (15) considered by Nakada (2002). The difference between this case and the results for $\beta \sim 0.008$ highlights the significance of incorporating the excess ellipticity of the planet into predictions of GIA-induced TPW. The range $0.06 < \beta < 0.010$ provides a reasonable estimate of the uncertainty associated with the excess ellipticity, and, accordingly, the zone between the dotted and dashed–dotted lines in Fig. 10 represents a measure of the uncertainty in the predicted TPW speed associated with GIA.

2.4 Rotational feedback

To complete our numerical predictions, we briefly revisit a recent area of active research related to GIA-induced TPW. Over the last decade there has been an increasing effort to model the feedback of TPW on a suite of geophysical signals associated with GIA, including relative sea-level histories (e.g. Han & Wahr 1989; Bills & James 1996; Milne & Mitrovica 1996, 1998; Sabadini & Vermeersen 1997; Peltier 1998; Johnston & Lambeck 1999; Mitrovica *et al.* 2001) and present-day rates of change of global sea level and its bounding surfaces (e.g. Mitrovica *et al.* 2001; Douglas & Peltier 2002).

Downloaded from https://academic.oup.com/gji/article/161/2/491/1995141 by guest on 21 August 2022

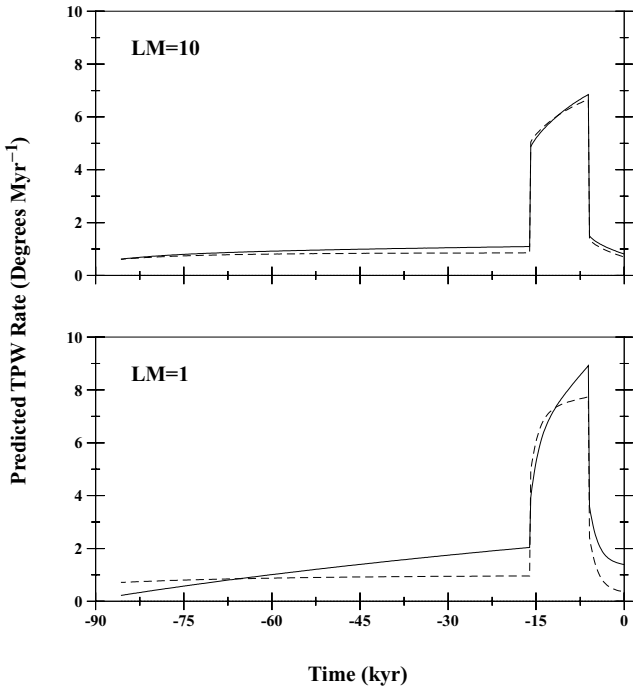

Figure 9. As Fig. 8, except showing the speed of the rotation pole.

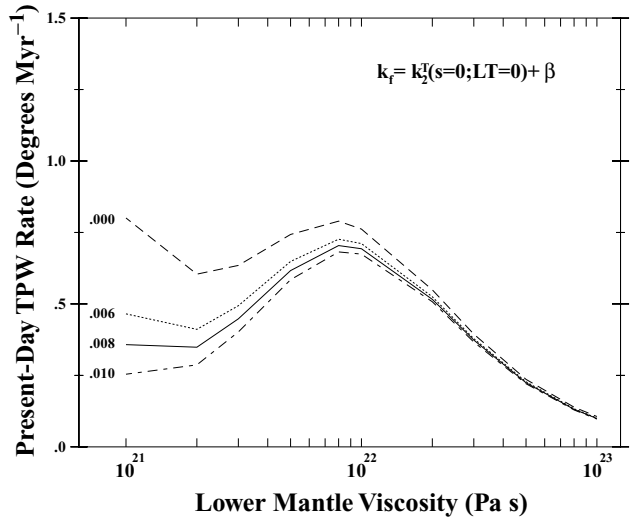

Figure 10. Summary of predictions of present TPW speed, as a function of the lower mantle viscosity (abscissa scale) of the earth model, generated using the time-domain Liouville equation (2). The predictions are generated using the new formulation (16) for the fluid Love number, and each line is distinguished on the basis of the choice for the parameter β (i.e. the contribution to k_f associated with the excess ellipticity of the Earth; as labelled at left). In particular, $\beta = 0.0$ (dashed line; i.e. the Nakada (2002) approach in eq. 15), 0.006 (dotted line), 0.008 (solid line; as assumed in eq. (16) following the difference between the 'observed' and 'Nakiboglu' results in Fig. 1), and 0.010 (dashed–dotted line). All calculations adopt an upper mantle viscosity of 10^{21} Pa s, and $LT = 100$ km. The surface mass load history is described in the text.

Milne & Mitrovica (1998) and Mitrovica *et al.* (2001) provide a theoretical formalism, based on viscoelastic Love number theory, for computing this TPW feedback. Once the Liouville equations are solved and a TPW path is established, the next step is to compute a time history of the changing centrifugal (or rotational driving) potential. This driving potential is then convolved, in time, with the appropriate viscoelastic tidal Green's functions (which are in turn computed from the appropriate combination of the $k_2^T(t)$ and $h_2^T(t)$ Love numbers, the latter not discussed here) to compute the observable of interest. Furthermore, in sea-level calculations, corrections are included to conserve the mass of the surface load.

For the present purposes, it suffices to define the perturbation to global sea level, $S(\theta, \phi, t)$, as the difference in perturbations to the geoid (or sea surface), $G(\theta, \phi, t)$, and the radial position of the solid surface (i.e. sea bottom), $R(\theta, \phi, t)$, i.e.

$$S(\theta, \phi, t) = G(\theta, \phi, t) - R(\theta, \phi, t). \tag{18}$$

In this case, relative sea-level histories, *RSL*, are obtained by referencing all perturbations in sea level to the present day:

$$RSL(\theta, \phi, t) = S(\theta, \phi, t) - S(\theta, \phi, t_p). \tag{19}$$

In the following we present predictions of *RSL* at a specific geographic site, as well as both global and site-specific predictions of the present-day rate of change of each of the fields in eq. (18). For the sake of simplicity, the predictions below do not include the effect of the changing water load on the sea-level predictions, since our intent is to focus only on the direct impact of the changing centrifugal potential. Full calculations, which include the ocean-loading term, will differ by those shown here by no more than ∼10 per cent.

In Fig. 11 we show plots with a format analogous to Figs 8 and 9; in this case, we present predictions of relative sea-level

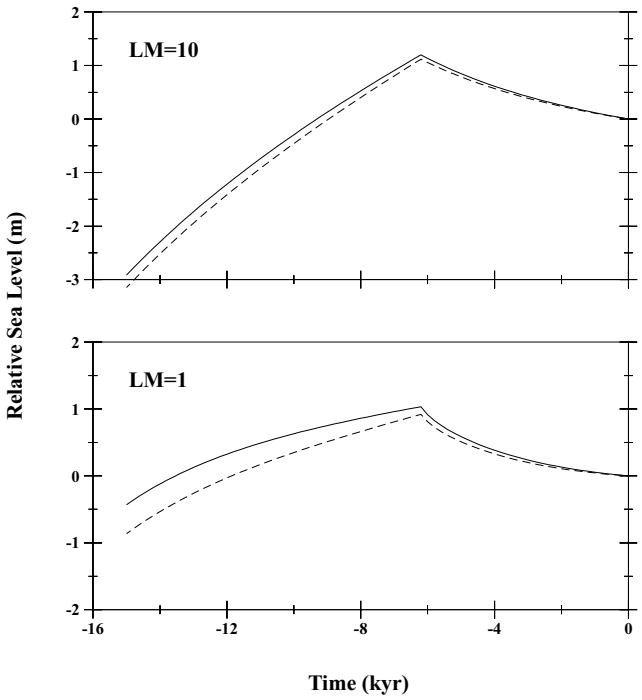

Figure 11. Predictions of relative sea-level change at a site in China (Tientsin, 39°N, 117.5°E), driven by load-induced perturbations in the rotation vector, over the last ∼15 kyr. The calculations neglect the relatively small contribution associated with rotation-driven redistribution of the ocean mass load. The predictions are generated using an earth model with a purely elastic lithosphere of thickness 100 km, an upper mantle viscosity of 10^{21} Pa s, and a lower mantle viscosity of either 10^{21} Pa s (bottom frame) or 10^{22} Pa s (top frame). In each frame the lines were generated using a time-domain form of the governing Liouville equation (2) with k_f given by: solid line—eq. (16) or (17); and dashed line—eq. (9) (i.e. the Liouville equation 11). The surface mass loading history is described, in detail, in the text.

Downloaded from https://academic.oup.com/gji/article/161/2/491/1995141 by guest on 21 August 2022

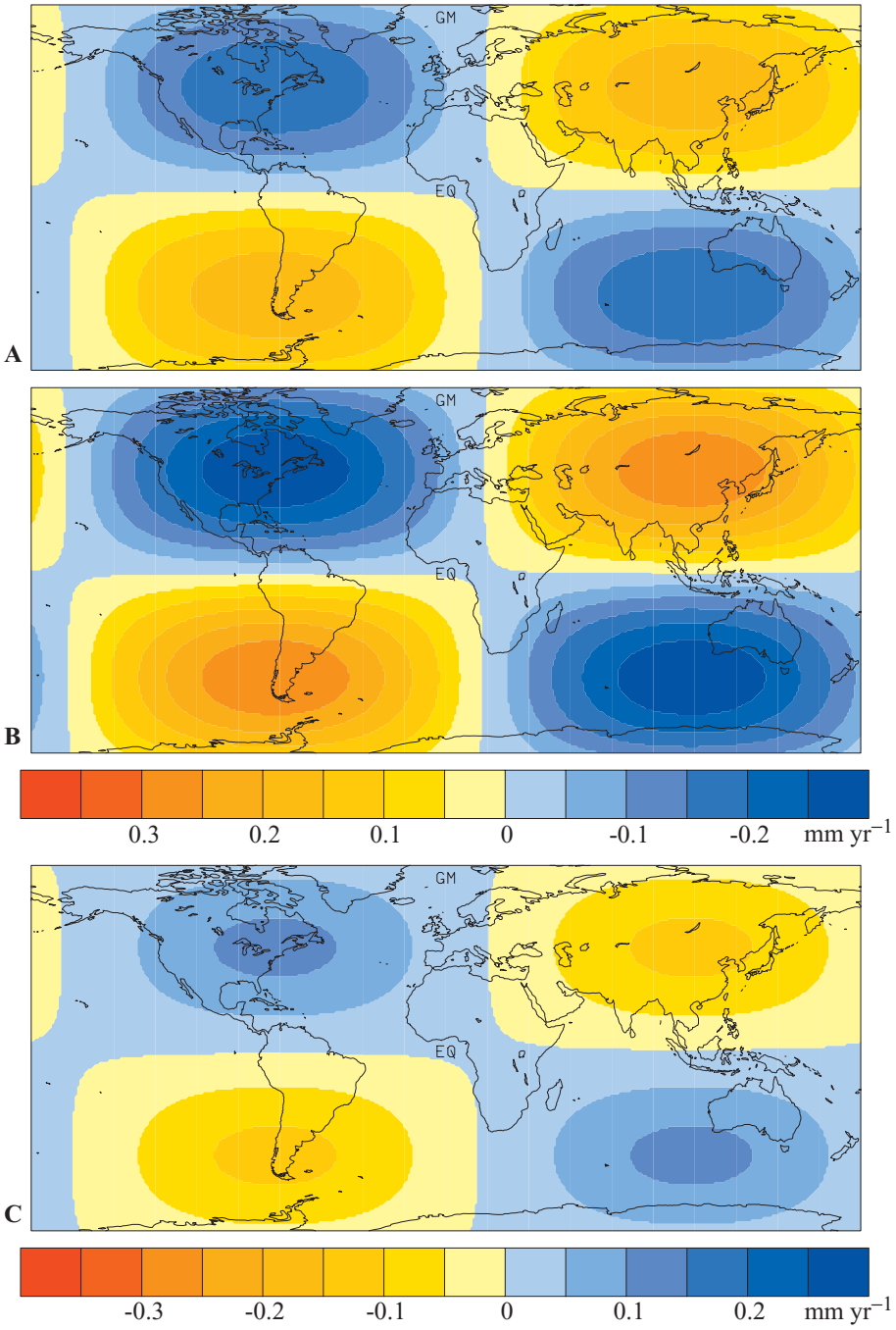

Figure 12. Predictions of present-day rates of change of (a) the geoid (or sea surface), (b) the solid surface, and (c) relative sea level, driven by load-induced perturbations in the rotation vector (i.e. the rotational feedback signal). The calculations neglect the relatively small contribution associated with rotation-driven redistribution of the ocean mass load. The predictions are generated using an earth model with a purely elastic lithosphere of thickness $LT = 100$ km, an upper mantle viscosity of 10^{21} Pa s, and a lower mantle viscosity of 2×10^{21} Pa s. Following eq. (18), the bottom frame represents the difference between the fields in the top two frames. The calculations all adopt the time-domain form of the governing Liouville equation (2) with k_f provided by eq. (16) or (17). The surface mass loading history is described, in detail, in the text.

change over the last ∼15 kyr at a site in China, Tientsin. The site was chosen because it was included in the study of Milne & Mitrovica (1998), where it was characterized by one of the largest amplitudes of TPW feedback on *RSL*. As before, the discrepancy between predictions associated with old (eq. 9) and new (eqs 16 or 17) expressions for k_f in the Liouville equation (2) are larger for the weak lower mantle viscosity case. However, even in this case, the difference in the predictions of RSL-change over the bulk of the period since the last glacial maximum (18 kyr ago) reaches only ∼0.5 m; this represents about 25 per cent of the peak-to-peak RSL feedback.

In Figs 12 and 13 we turn our attention to predictions of rotational feedback on present-day rates of change of sea level and its bounding surfaces. Fig. 12 presents global plots of the feedback in the fields (from top to bottom) $\dot{G}(\theta, \phi, t_p)$, $\dot{R}(\theta, \phi, t_p)$ and $\dot{S}(\theta, \phi, t_p)$, computed using $LT = 100$ km, and a lower mantle viscosity of

Downloaded from https://academic.oup.com/gji/article/161/2/491/1995141 by guest on 21 August 2022

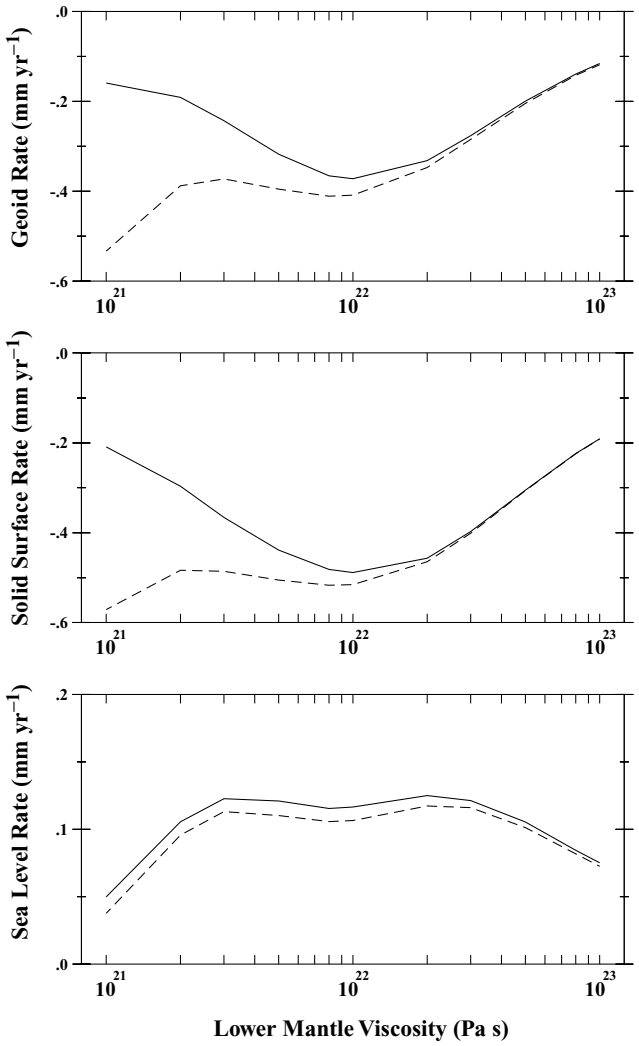

Figure 13. Predictions of present-day rates of change of (top) the geoid (or sea surface), (middle) the solid surface and (bottom) the relative sea level, at a site on the east coast of the US (Clinton, 41.2° N, 287.5° E), driven by load-induced perturbations in the rotation vector (i.e. the rotational feedback signal). This site is close to a maximum in the associated global fields, as is evident from Fig. 12. The predictions are shown as a function of the adopted lower mantle viscosity; the upper mantle viscosity is set to 10^{21} Pa s, while the thickness of the purely elastic lithosphere is taken to be $LT = 100$ km. In each frame the lines were generated using a time-domain form of the governing Liouville equation (2) with k_f provided by: solid line—eq. (16) or (17); and dashed line—eq. (9) (i.e. the Liouville equation 11). The surface mass loading history is described, in detail, in the text.

2×10^{21} Pa s. These predictions are based on k_f given by our new theory (eq. 16 or 17). As has been noted elsewhere (e.g. Han & Wahr 1989; Milne & Mitrovica 1996), the fields are dominated by a degree-two and order-one harmonic, and the sea-level prediction, since it is the difference between two bounding surfaces that approximately track one another (see the top two frames of the figure), shows a smaller amplitude than the geoid and solid-surface displacement fields (Mitrovica *et al.* 2001). The amplitude of the sea-level rate is ∼0.1 mm yr^{-1}, which is relatively small compared with fluctuations in sea level recorded by tide gauges; the geoid (sea surface) and solid-surface rates reach ∼0.2 mm yr^{-1} and ∼0.3 mm yr^{-1}, respectively.

In Fig. 13 we repeat the calculation in Fig. 12 for a suite of lower mantle viscosities. Specifically, we show present-day rates at a site on the US east coast, Clinton, located near the peak of the (2, 1) geometry in Fig. 12. Within each frame, we present predictions of the TPW feedback signal computed using a fluid Love number given by eqs (16 or17; solid line) and (9; dashed line). These results indicate that the formulation adopted to specify the background oblateness of the planet has little impact on the prediction of the TPW feedback on the present-day sea-level rate (bottom frame); however, the discrepancy associated with the predicted geoid and solid-surface rate mirrors the differences between the present-day TPW speed predictions in Figs 2 and 5, and can thus be large for the class of models with relatively weak lower mantle viscosity. Indeed, for ν_{LM} values in the range of 10^{21} to 3×10^{21} Pa s, the approximation (9) leads to an overestimate of a factor of ∼2 to 4 in the TPW feedback on these fields.

Peltier (2004) has recently presented predictions of the GIA contribution to present-day geoid rates using a preferred earth model (VM2) characterized by a lower mantle viscosity varying in the range 2–3$\times 10^{21}$ Pa s. These predictions, motivated by the impending availability of high-precision GRACE satellite constraints, were based on the traditional TPW theory. We conclude that the large (2,1) TPW feedback signal evident in them (Peltier 2004; fig. 22) is overestimated by at least a factor of ∼2.

3 THE PHYSICS OF GIA-INDUCED TPW: A SUMMARY

The numerical predictions summarized above have highlighted subtle, and previously unappreciated, issues related to the rotational stability of an ice-age Earth. The viscoelastic GIA problem has important similarities to, and significant differences from, classical treatments of the rotational stability of rotating inviscid planets (Gold 1955; Goldreich & Toomre 1969; Willemann 1984). In this section we provide a general physical framework for understanding the traditional and new GIA predictions within the context of these earlier seminal studies. Our discussion will be supported by the schematic illustrations in Fig. 14.

Traditional predictions of GIA-induced TPW assume no underlying geodynamic contributions to the inertia tensor. That is, no account is taken, for example, of any excess ellipticity driven by mantle convective flow. Furthermore, these predictions assume that the equilibrium rotating form of the planet is a function of the thickness of the elastic lithosphere. Conceptually, the latter assumes that the equilibrium form was established by first starting with a non-rotating model having an elastic lid of thickness LT and then considering the infinite-time, equilibrium form generated by imposing the present rotation rate onto this idealized model. With this in mind, we can consider two subcases: $LT = 0$ and $LT \neq 0$. These are illustrated in Figs 14(a) and (b), respectively, with the left-most panel in each case showing the initial, equilibrium form.

For the first of these cases, $LT = 0$, one may still suppose that the lithosphere acts as a zone of high viscosity in its response both to the ice load and to the change in centrifugal forcing. Now suppose a surface mass loading is instantaneously applied, for example an ice load upon Hudson Bay (Fig. 14a2). The rotation axis responds by moving away from Hudson Bay. (In Fig. 14 the green arrows acting on the rotation pole refer to the TPW driven by the 'green' surface mass load dimple.) That is, the adjustment will tend to move the ice load towards the point furthest from the rotation axis, the equator. Initially, though, the rotation axis will not move very far, because as

Downloaded from https://academic.oup.com/gji/article/161/2/491/1995141 by guest on 21 August 2022

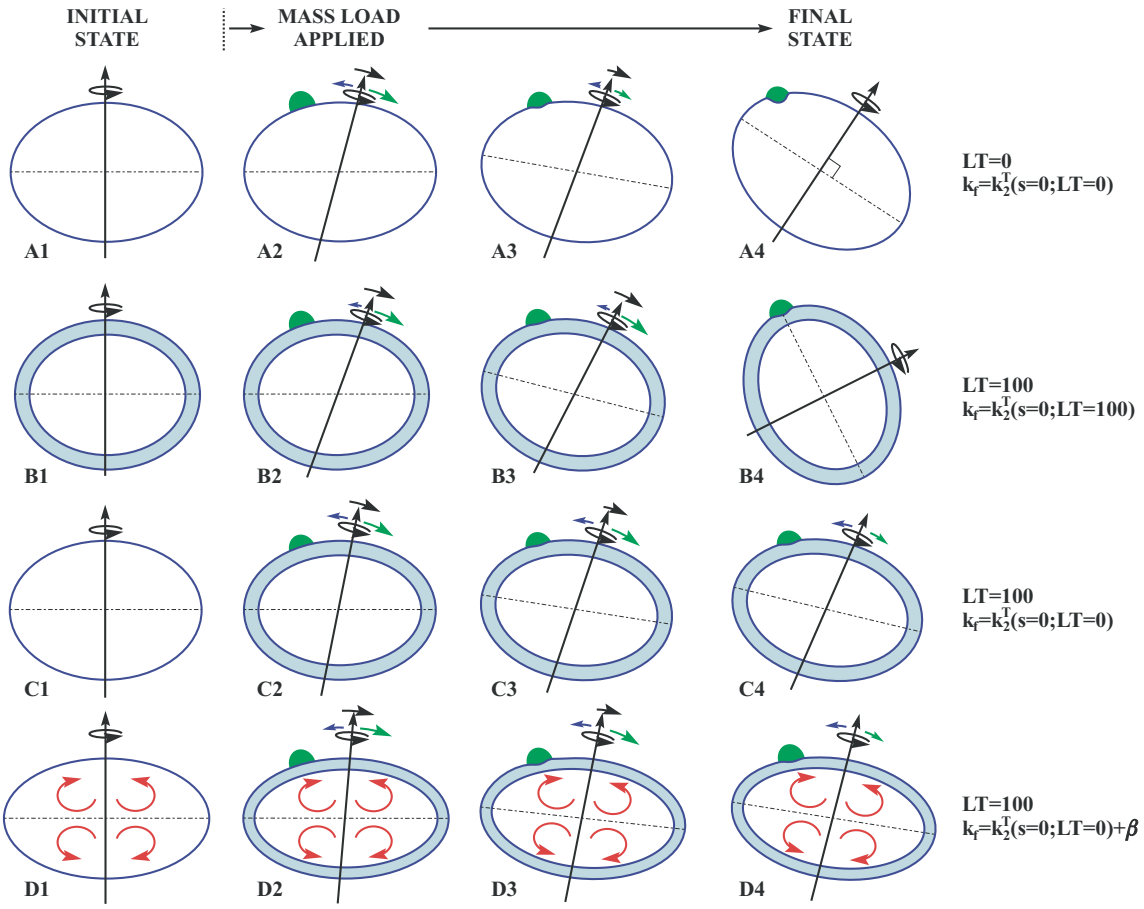

Figure 14. Schematic illustrating the physics of GIA-induced TPW for various modelling scenarios. Details of the figure are provided in the text. On the right margin, the *LT* value refers to the thickness of the elastic lithosphere associated with the response to both a surface mass load and rotational driving potential (shaded blue region superimposed on the earth models); furthermore, k_f is the fluid Love number that governs the equilibrium background form of the planet (β is the contribution from excess ellipticity; see eq. 16). The long and straight black arrow passing through the models is the rotation axis. The green dimple on the various frames represents a surface mass load, which is subject to some degree of isostatic compensation, while the red arrows within the planetary interior denote any underlying geodynamic processes (e.g. mantle convection). The green arrow represents the TPW signal driven by the surface mass loading, while the blue arrow is the TPW signal connected to any remnant bulge effects (e.g. due to an unrelaxed rotational form subsequent to a TPW event, or long-term excess ellipticity).

it gets displaced the large equatorial (i.e. C-A) bulge moves off the equator, and this will induce a restoring force on the rotation axis. (In Fig. 14 the blue arrow acting on the rotation pole refers to the TPW driven by any unrelaxed rotational bulge.) In time, the equatorial bulge viscously adjusts to the perturbation in the centrifugal force caused by the displaced rotation axis, rearranging mass towards the new equator; the axis is then free to shift further away from the ice load (Gold 1955; Goldreich & Toomre 1969). At the same time, of course, the Earth beneath the ice load relaxes viscously, so that the axis is not pushed away from the load quite so strongly. This trend is reflected by the gradual subsidence towards isostatic equilibrium of the surface mass load in Fig. 14(a) and the gradial diminution of the load-induced TPW signal (green arrow).

In the limit of infinite time, the load-induced forcing will vanish since the surface mass load will be perfectly compensated when $LT = 0$. In addition, at infinite time the rotationally induced bulge will have relaxed completely to the orientation of the new rotation axis, and thus the ellipsoidal form in Fig. 14(a4) is simply a reoriented version of the form in Fig. 14(a1). Thus, both the green and blue arrows have disappeared in the final, equilibrium state (Fig. 14a4). At this stage, the rotation pole will have shifted a finite, but non-zero amount, governed by the balance between the two processes of viscous relaxation. Furthermore, the rate of polar motion will have fallen off to zero. This result can also be inferred, mathematically, from the Laplace transform inversion of eq. (12), given in the Appendix. In the case of a viscous lithosphere, $k_2^L(s = 0) = -1$, and thus the load compensation term $D_2 = 0$. Thus, the response is well behaved in the long time limit since the linear term in time, t, in eq. (26) vanishes. In any event, at infinite time, the pole has not returned to where it started, even though the ice load is completely compensated. Without any underlying geodynamic contributions to the inertia tensor, or a remnant rotational bulge, the Earth has no preferred location for its rotation axis.

Next, consider an earth model in which $LT \neq 0$ (Fig. 14b), and where the fluid Love number is computed using eq. (9) with this same non-zero lithospheric thickness. In this case, there is still a non-zero load imposed on the planet at infinite time, since the surface mass load is never fully compensated (Fig. 14b2–4). In contrast, the equatorial bulge can, at least in principle, relax completely to a change in the orientation of the rotation axis. That is, there will be no remnant bulge since the model used to compute the

Downloaded from https://academic.oup.com/gji/article/161/2/491/1995141 by guest on 21 August 2022

background oblateness (i.e. $k_2^{\rm T}(s = 0; LT)$) is the same as the model used to compute the response to the driving potential. Thus, at infinite time, the rotation axis will continue to be pushed away from the load, but there will be no residual bulge to supply an opposing force. This can again be confirmed mathematically with reference to eq. (26): when $LT \neq 0$, $D_2 = 1 + k_2^{\rm L}(s = 0) \neq 0$, and thus the displacement of the pole increases linearly in time while the rate of motion does not converge to 0. In a non-linear theory, the displacement would, of course, cease when the load reaches the equator, as in Fig. 14(b4).

This example ($LT \neq 0$) is consistent with the basic physics addressed by Gold (1955) and Goldreich & Toomre (1969), and we arrive at the same conclusion: the rotation of an earth model in the presence of an uncompensated mass load, *and* in the case where the equatorial bulge can relax completely, is unstable. We note that Gold (1955) and Goldreich & Toomre (1969) arrived at this conclusion using a hybrid model that was hydrostatic in its response to a perturbation in rotation and rigid in its response to a surface mass load.

In contrast to Fig. 14(b), our first scenario (Fig. 14a) provides an extension of the Goldreich & Toomre (1969) physics to the case where there is also perfect, at infinite time, compensation of the surface mass load (since $LT = 0$). In this case, the compensation acts to stabilize the rotation pole. The increased stability of the pole as $LT \rightarrow 0$ is the key to understanding the trends for different values of LT in the 'traditional' calculations of Fig. 2(a) (see also the discussion related to Fig. 4b).

Next we turn to the case in which the background oblateness is consistent with an entirely fluid planet, while the Earth's response to the surface mass load and centrifugal driving potential over GIA timescales involves an elastic lithosphere of thickness $LT \neq 0$ (Fig. 14c). We continue to assume that there are no underlying geodynamic contributions to the background oblateness. In contrast to the above, $LT \neq 0$ scenario (row b), we are thus presuming either: (1) that the equilibrium form is hydrostatic and that it was set early in Earth history when there was no lithosphere; or (2) that, while the lithosphere might maintain elastic strength over GIA timescales and stress levels, it might not do so in the presence of much larger, and long-term, rotation. Regardless, this scenario is consistent with the case in which expression (15) is used within the Liouville equations.

The final GIA-induced polar wander in this case (Fig. 14c4) is characterized by a finite, but non-zero, shift, and the rate of polar motion converges to zero. The reason is that, while the rotation axis continues to be pushed away from the incompletely compensated load (the load-induced, green arrow, TPW signal in Fig. 14(c) does not vanish), the equatorial bulge cannot relax completely to the change in pole position. That is, there will be a remnant rotational bulge, and eventually a final, equilibrium balance at non-zero distance from the original pole position is achieved. The incomplete relaxation of the bulge is a consequence of the fact that the background oblateness is hydrostatic, while the response to the TPW is, in contrast, subject to a perfectly elastic lithosphere.

This third scenario can be considered an extension of the Goldreich & Toomre (1969) results to the case where the rotational bulge is not permitted to relax completely; see Willemann (1984) for a discussion of the final, equilibrium state in this scenario (Fig. 14c4). The stabilization of the rotation pole associated with this extension (Fig. 14c4 compared with Fig. 14b4) is the underlying reason why the prediction of GIA-induced TPW rate based on expression (15) (dashed line, Fig. 10) has lower amplitude than the traditional prediction (solid line; Fig. 2) based on eq. (9), where both adopt $LT = 100$ km in predicting the response to the surface mass load and TPW.

The third scenario highlights a general principle. In the case where the lithosphere has elastic strength in response to a changing surface mass load and rotational driving potential, the stability of the rotation pole at infinite time (i.e. the displacement of the pole to a position less than 90° from the imposed load) requires that the background oblateness be larger than the equilibrium form obtained after a change in the pole position. That is, the fluid Love number has to be greater than $k_2^{\rm T}(s = 0; LT)$ in the symbolism adopted the text. The scenario in Fig. 14(c) achieves this by having the background form coincide with the hydrostatic state of the planet; from Fig. 1, we note again that $k_2^{\rm T}(s = 0; LT = 0) > k_2^{\rm T}(s = 0; LT \neq 0)$.

An additional way of ensuring that the background oblateness be larger than the post-TPW equilibrium form is to incorporate an excess ellipticity of the planet originating from a static, relative to the timescale of GIA, geodynamic process such as mantle convection. This case is described by eqs (16) and (17) and it is the subject of Fig. 14(d). At infinite time, when $LT \neq 0$, the uncompensated surface mass load will continue to push the pole away, while the incomplete relaxation of the rotational bulge will resist this trend (as in Fig. 14c4). In addition, the underlying geodynamic contribution, that is the convection-induced excess ellipticity, will not relax, and will thus contribute a further, stabilizing influence on the pole position (compare Figs 14d4 and c4). As before, a balance will be achieved; the net pole displacement will diminish as the adopted level of excess ellipticity increases. Indeed, the monotonically stabilizing effect of increasing the excess ellipticity is clearly evident in Fig. 10. This is a further extension to the basic physics of a rotating earth elucidated by Gold (1955) and Goldreich & Toomre (1969).

A final scenario is worthy of a brief comment. Let us return to the case where the earth model has no elastic strength in the presence of a surface mass or rotation-induced potential loading (i.e. $LT = 0$). In the case of a hydrostatic background form, i.e. when there is no underlying geodynamic contribution of an excess ellipticity, the scenario of Fig. 14(a) indicates that the pole will ultimately be stabilized by the complete (at infinite time) compensation of the surface mass load. What if we introduced an excess ellipticity into the $LT = 0$ scenario of Fig. 14(a), or, equivalently, what if we set $LT = 0$ in the scenario treated in Fig. 14(d)? In this case, the pole would return, at infinite time, to its initial location prior to loading, since the geodynamically supported excess flattening will not relax, except perhaps over timescales that are long relative to the geodynamic process. The geodynamic contributions provide a preferred location for the rotation axis in this scenario, and the surface mass loading introduces only a transient perturbation in the pole location.

4 FINAL REMARKS

The prediction of GIA-induced variations in the Earth's rotation axis has a modern history that dates back to theoretical work, based on viscoelastic normal-mode theory, from the early 1980s. The stability of the rotation pole on a viscoelastic planet loaded by a surface mass depends both on the deformational response of the planet to the mass and (associated) rotational load as well as on the background oblateness upon which this deformation is applied. The main conclusion of this paper is that traditional GIA calculations have erred in using a strongly model-dependent prediction of this background form, rather than a (model-independent) oblateness that reflects the excess ellipticity of the planet from its hydrostatic form. The

Downloaded from https://academic.oup.com/gji/article/161/2/491/1995141 by guest on 21 August 2022

traditional approximation is, in practice, embedded in an assumption that the so-called fluid Love number, $k_{\rm f}$, appearing in the linearized Euler, or Liouville equations may be replaced by the fluid ($s = 0$) limit of the s-domain $k_2^{\rm T}$ tidal Love number computed for the same earth model as used to predict the load-induced deformation. As we have discussed, this assumption introduces an error that is a strong function of the thickness of the elastic lithosphere in the adopted earth model.

We propose an alternative theoretical treatment, where the fluid Love number is based on either (1) the hydrostatic ($LT = 0$, $s = 0$) form computed using viscoelastic Love number suitably augmented to include the independently inferred excess ellipticity of the Earth (eq. 16); or (2) the observed (i.e. present-day) oblateness and rotation rate of the planet with a scaling applied to account for errors in the Love number theory adopted to compute the response of the earth model to a mass load or centrifugal forcing (eq. 17). These treatments ultimately lead to identical expressions for $k_{\rm f}$; predictions based upon them show a more stable rotation pole, relative to traditional predictions, with lower predicted amplitudes for present-day TPW speed. Significantly, the new results do not show sensitivities, for example to the adopted lithospheric thickness or rheology, that have characterized previous studies and that have heretofore defied explanation.

It is not uncommon within the GIA literature to compute Love numbers using highly simplified earth models which, in some bulk sense, approximate the Earth's elastic and density structure. Predictions of TPW that mix calculations of $k_2^{\rm T}(s)$ with the observed value of the fluid Love number, $k_{\rm f}$, would, in this case, be subject to potentially large errors. Our new formulations (16) and (17) ensure, either explicitly or implicitly, that the denominator and numerator of the ratio $k_2^{\rm T}(s)/k_{\rm f}$ appearing in the Liouville equation differ by the excess ellipticity of the planet as the fluid limit is approached. Thus, they also have the advantage of limiting the error incurred in TPW predictions that adopt such simplified earth models.

We have computed a suite of predictions of the feedback of TPW on geophysical observables related to global sea-level change and its bounding surfaces. These predictions indicate that previous results, like those of present-day TPW speed, have overestimated the amplitude of the feedback. We conclude that future predictions of GIA-induced TPW, and related effects, in applications as diverse as the inference of mantle structure and present-day cryospheric mass balance, should adopt the more accurate theory described here. While this conclusion is based on spherically symmetric calculations, it will also hold for a new generation of predictions based on 3-D earth models.

ACKNOWLEDGMENTS

We thank Erik Ivins and Bruce Bills for constructive reviews, and Masao Nakada, Michael Manga and Taylor Perron for numerous discussions related to this work. Support for this research was provided by NSERC, NSF grant EAR-0087567, NASA grant NAG-12380, the David and Lucile Packard Foundation, the Miller Institute for Basic Research in Science, and the Canadian Institute for Advanced Research.

REFERENCES

Bills, B.G. & James, T.S., 1996. Late Quaternary variations in relative sea level due to glacial cycle polar wander, *Geophys. Res. Lett.,* **23,** 3023–3026.

Douglas, B.C, & Peltier, W.R., 2002. The puzzle of global sea-level rise, *Physics Today,* **55,** 35–40.

Dziewonski, A.M. & Anderson, D.L., 1981. Preliminary reference Earth model (PREM), *Phys. Earth planet. Inter.,* **25,** 297–356.

Gasperini, P., Sabadini, R. & Yuen, D.A., 1986. Excitation of the Earth's rotational axis by recent glacial discharges, *Geophys. Res. Lett.,* **13,** 533–536.

Gold, T., 1955. Instability of the Earth's axis of rotation, *Nature,* **175,** 526–529.

Goldreich, P. & Toomre, A., 1969. Some remarks on polar wandering, *J. geophys. Res.,* **74,** 2555–2567.

Han, D. & Wahr, J., 1989. Post-glacial rebound analysis for a rotating Earth, in *Slow Deformations and Transmission of Stress in the Earth, AGU Mono. Series 49,* pp. 1–6, eds Cohen, S. & Vanicek, P. , AGU, Washington, DC, USA.

Ivins, E.R., Sammis, C.G. & Yoder, C.F., 1993. Deep mantle viscosity structure with prior estimate and satellite constraint, *J. geophys. Res.,* **98,** 4579–4609.

Johnston, P. & Lambeck, K., 1999. Postglacial rebound and sea level contributions to changes in the geoid and the Earth's rotation axis, *Geophys. J. Int.,* **136,** 537–558.

Lambeck, K., 1980. *The Earth's Variable Rotation: Geophysical Causes and Consequences,* Cambridge Univ. Press, London.

Milne, G.A. & Mitrovica, J.X., 1996. Postglacial sea-level change on a rotating Earth: first results from a gravitationally self-consistent sea-level equation, *Geophys. J. Int.,* **126,** F13–F20.

Milne, G.A. & Mitrovica, J.X., 1998. Postglacial sea level change on a rotating Earth, *Geophys. J. Int.,* **133,** 1–10.

Milne, G.A., Mitrovica, J.X. & Davis, J.L., 1999. Near-field hydro-isostasy: the implementation of a revised sea-level equation, *Geophysic. J. Int.,* **139,** 464–482.

Mitrovica, J.X. & Milne, G.A., 1998. Glaciation-induced perturbations in the Earth's rotation: A new appraisal, *J. geophys. Res.,* **103,** 985–1005.

Mitrovica, J.X. & Peltier, W.R., 1989. Pleistocene deglaciation and the global gravity field, *J. geophys. Res.,* **94,** 13 651–13 671.

Mitrovica, J.X. & Peltier, W.R., 1993. Present-day secular variations in the zonal harmonics of the Earth's geopotential, *J. geophys. Res.,* **98,** 4509–4526.

Mitrovica, J.X., Milne, G.A. & Davis, J.L., 2001. Glacial isostatic adjustment on a rotating Earth, *Geophys. J. Int.,* **147,** 562–579.

Mound, J.E., Mitrovica, J.X. & Forte, A.M., 2003. The equilibrium form of a rotating earth with an elastic shell, *Geophys. J. Int.,* **152,** 237–241.

Munk, W.H., 2002. Twentieth century sea level: An enigma, *Proc. Nat. Acad. Sci.,* **99,** 6550–6555.

Munk, W.H. & MacDonald, G.J.F., 1960. *The Rotation of the Earth,* Cambridge Univ. Press, New York.

Nakada, M., 2000. Effects of the viscoelastic lithosphere on polar wander speed caused by the late Pleistocene glacial cycles, *Geophys. J. Int.,* **143,** 230–238.

Nakada, M., 2002. Polar Wander caused by the Quaternary glacial cycles and the fluid Love number, *Earth planet. Sci. Lett.,* **200,** 159–166.

Nakiboglu, S.M., 1982. Hydrostatic theory of the Earth and its mechanical implications, *Physics Earth planet. Inter.,* **28,** 302–311.

Nakiboglu, S.M. & Lambeck, K., 1980. Deglaciation effects upon the rotation of the Earth, *Geophys. J. R. astr. Soc.,* **62,** 49–58.

Peltier, W.R., 1974. The impulse response of a Maxwell Earth, *Rev. Geophys.,* **12,** 649–669.

Peltier, W.R., 1976. Glacial isostatic adjustment, 2, The inverse problem, *Geophys. J. R. astr. Soc.,* **46,** 669–706.

Peltier, W.R., 1988. Global sea level and earth rotation, *Science,* **240,** 895–901.

Peltier, W.R., 1998. Postglacial variations in the level of the sea: Implications for climate dynamics and solid-Earth geophysics, *Rev. Geophys.,* **36,** 603–689.

Peltier, W.R., 2004. Global glacial isostasy and the surface of the ice-age Earth: The ICE-5G (VM2) model and GRACE, *Annu. Rev. Earth planet. Sci.,* **32,** 111–149.

Downloaded from https://academic.oup.com/gji/article/161/2/491/1995141 by guest on 21 August 2022

Peltier, W.R. & Jiang, X., 1996. Glacial isostatic adjustment and Earth rotation: Refined constraints on the viscosity of the deepest mantle, *Geophys. J. Int.,* **101,** 3269–3290.
Peltier, W.R. & Wu, P., 1983. Continental lithospheric thickness and deglaciation induced true polar wander, *Geophys. Res. Lett.,* **10,** 181–184.
Sabadini, R. & Peltier, W.R., 1981. Pleistocene deglaciation and the Earth's rotation: implications for mantle viscosity, *Geophys. J. R. astr. Soc.,* **66,** 553–578.
Sabadini, R. & Vermeersen, L.L.A., 1997. Ice-age cycles: Earth's rotation instabilities and sea-level changes, *Geophys. Res. Lett.,* **24,** 3041–3044.
Spada, G., Sabadini, R., Yuen, D.A. & Ricard, Y., 1992. Effects on post-glacial rebound from the hard rheology in the transition zone, *Geophys. J. Int.,* **109,** 683–700.
Tromp, J. & Mitrovica, J.X., 1999. Surface loading of a viscoelastic Earth - II. Spherical models, *Geophys. J. Int.,* **137,** 856–872.
Tushingham, A.M. & Peltier, W.R., 1991. ICE-3G: A new global model of late Pleistocene deglaciation based on geophysical predictions of post-glacial relative sea level change, *J. geophys. Res.,* **96,** 4497–4523.
Vermeersen, L.L.A. & Sabadini, R., 1996. Significance of the fundamental mantle relaxation mode in polar wander simulations, *Geophys. J. Int.,* **127,** F5–F9.
Vermeersen, L.L.A., Fournier, A. & Sabadini, R., 1997. Changes in rotation induced by Pleistocene ice masses with stratified analytical Earth models, *J. geophys. Res.,* **102,** 27 689–27 702.
Willemann, R.J., 1984. Reorientation of planets with elastic lithospheres, *Icarus,* **60,** 701–709.
Wu, P. & Peltier, W.R., 1982. Viscous gravitational relaxation, *Geophys. J. R. astr. Soc.,* **70,** 435–485.
Wu, P. & Peltier, W.R., 1984. Pleistocene deglaciation and the Earth's rotation: A new analysis, *Geophys. J. R. astr. Soc.,* **76,** 753–792.
Yuen, D.A. & Sabadini, R., 1985. Viscosity stratification of the lower mantle as inferred from the $\dot{J}_2$observation, *Ann. Geophys.,* **3,** 647–654.
Yuen, D.A., Sabadini, R. & Boschi, E., 1982. Viscosity of the lower mantle as inferred from rotational data, *J. geophys. Res.,* **87,** 10 745–10 762.

APPENDIX A:

Wu & Peltier (1984; eqs 79–80) inverted the s-domain Liouville equation (12) to obtain the following time-domain solution:

$$\mathbf{m}(t) = \frac{\Omega}{A\sigma_o}\left\{ D_1 \mathbf{I}^{\mathrm{L}}(t) + D_2 \int_{t=0}^{t} \mathbf{I}^{\mathrm{L}}(t')\,dt' + \sum_{k=1}^{K-1} E_k \left[\mathbf{I}^{\mathrm{L}}(t) * \exp(-\lambda_k t)\right]\right\}, \quad (20)$$

where σ_o is the wobble frequency on the deformable earth,

$$D_1 = 1 + k_2^{\mathrm{L,E}}, \quad (21)$$

$$D_2 = [1 + k_2^{\mathrm{L}}(s=0)]\frac{\prod_{l=1}^{K} s_l}{\prod_{l=1}^{K-1} \lambda_l}, \quad (22)$$

and

$$E_k = -\frac{\frac{1+k_2^{\mathrm{L}}(s=0)}{\lambda_k}\prod_{l=1}^{K}(s_l - \lambda_k) + \sum_{j=1}^{K} \frac{r'_j}{s_j} \prod_{l\neq j}^{K}(s_l - \lambda_k)}{\prod_{q\neq i}^{K-1}(\lambda_q - \lambda_k)}. \quad (23)$$

The inverse decay times λ_i represent the $K-1$ roots of the equation

$$Q_{K-1}(s) = \sum_{j=1}^{K} g_j^{\mathrm{T}} \prod_{i\neq j}^{K}(s + s_i), \quad (24)$$

where

$$g_j^{\mathrm{T}} = \frac{r''_j/s_j}{\sum_{q=1}^{K} r''_q/s_q}. \quad (25)$$

In the text we discuss the case of a single load component applied and retained on the Earth at some time t_0. In this case we can write $\mathbf{I}^{\mathrm{L}}(t) = \mathbf{I}^{\mathrm{L}} H(t - t_0)$, where H is the Heaviside step function. Using the above equations, the rotational response to the loading is given by

$$\mathbf{m}(t) = \frac{\Omega}{A\sigma_o}\left\{ D_1 \mathbf{I}^{\mathrm{L}} + D_2 \mathbf{I}^{\mathrm{L}} t + \mathbf{I}^{\mathrm{L}} \sum_{k=1}^{K-1} \frac{E_k}{\lambda_k}[1 - \exp(-\lambda_k t)]\right\}. \quad (26)$$

Downloaded from https://academic.oup.com/gji/article/161/2/491/1995141 by guest on 21 August 2022